AD_____

Award Number: DAMD17-00-1-0195

TITLE: Tactile Mapping of Breast Palpation for Diagnosis, Documentation, and Training

PRINCIPAL INVESTIGATOR: Rujirutana Srikanchana

CONTRACTING ORGANIZATION: The Catholic University of America
Washington, DC 20064

REPORT DATE: September 2002

TYPE OF REPORT: Annual Summary

PREPARED FOR: U.S. Army Medical Research and Materiel Command
Fort Detrick, Maryland 21702-5012

REPORT DOCUMENTATION PAGE

Form Approved
OMB No. 074-0188

1. AGENCY USE ONLY (Leave blank)	2. REPORT DATE	3. REPORT TYPE AND DATES COVERED
	September 2002	Annual Summary (1 Sep 01 - 31 Aug 02)

4. TITLE AND SUBTITLE
Tactile Mapping of Breast Palpation for Diagnosis, Documentation, and Training

5. FUNDING NUMBERS
DAMD17-00-1-0195

6. AUTHOR(S):
Rujirutana Srikanchana

7. PERFORMING ORGANIZATION NAME(S) AND ADDRESS(ES)
The Catholic University of America
Washington, DC 20064
E-Mail:
55srikan@pluto.ee.cua.edu

8. PERFORMING ORGANIZATION REPORT NUMBER

9. SPONSORING / MONITORING AGENCY NAME(S) AND ADDRESS(ES)
U.S. Army Medical Research and Materiel Command
Fort Detrick, Maryland 21702-5012

10. SPONSORING / MONITORING AGENCY REPORT NUMBER

11. SUPPLEMENTARY NOTES

12a. DISTRIBUTION / AVAILABILITY STATEMENT
Approved for Public Release; Distribution Unlimited

12b. DISTRIBUTION CODE

13. Abstract *(Maximum 200 Words)* ***(abstract should contain no proprietary or confidential information)***

Palpation by clinicians is an effective examination frequently performed for breast cancer detection and treatment monitoring. The most common symptom of breast cancer is a lump, and studies show that the majority of breast cancers are found by palpation. The primary goal of this project is to develop a tactile mapping system that can quantitatively measure the location and applied forces in breast palpation, and the tactile features of detected breast lumps. By combining the knowledge of vision based neural networks, tactile sensing technology is integrated for the investigation of soft tissue interaction with tactile/force sensor, where the hard inclusion (breast lump) can be characterized through neural network learning capabilities, instead of using a simplified complex biomechanics model with many heuristic assumptions. Through a nonlinear soft tissue analysis by the neural networks, the system can accurately characterize and document breast lumps. These maps will serve as an objective documentation of palpable lesions for future comparative examinations.

14. SUBJECT TERMS	15. NUMBER OF PAGES
breast cancer, palpation, tactile mapping	35
	16. PRICE CODE

17. SECURITY CLASSIFICATION OF REPORT	18. SECURITY CLASSIFICATION OF THIS PAGE	19. SECURITY CLASSIFICATION OF ABSTRACT	20. LIMITATION OF ABSTRACT
Unclassified	Unclassified	Unclassified	Unlimited

Table of Contents

INTRODUCTION:

Palpation by clinicians is an effective examination frequently performed for breast cancer detection and monitoring treatment. The most common symptom of breast cancer is a lump, and studies show that the majority of breast cancers are found by palpation. The primary goal of this project is to develop a tactile mapping system that can quantitatively measure the location and applied forces in breast palpation, and the tactile features of detected breast lumps. By combining the knowledge of vision based neural networks, tactile sensing technologies are integrated for the investigation of soft tissue interaction with tactile/force sensors, where the hard inclusion (breast lump) can be characterized through neural network learning capabilities, instead of using a simplified complex biomechanics model with many heuristic assumptions. Through a nonlinear soft tissue analysis by the neural network, the system can accurately characterize and document breast lumps. These maps will serve as an objective documentation of palpable lesions for future comparative examinations. Limited laboratory experimental evaluation has been conducted to collect preliminary data that will form a full-scale Task II research plan. Our considerable efforts in the Task II are

- To evaluate the sensitivity and reproducibility of the TMD system based on the feedback from the model-based laboratory evaluation and preliminary expert evaluation.
- To design suitable neural network based intelligence system for tactile signal interpretation
- To develop a training algorithms and computer interpretation codes.

BODY:

In the first year of this award, we have conducted a systematic study to adapt new tactile sensing technologies to the needs of improving physical breast examination, to gather preliminary data regarding potential clinical applications, and to advance the fundamental understanding of palpation. We established that an existing tactile sensor array and related force measurement technologies could be modified specifically for use as a tactile mapping device (TMD) and could be adapted for robotic medical sensing applications [3,4,5]. We applied the TMD to various educational models, which allowed the collection of sufficient tactile images.

In the second year of this award, we have taken the feedback from the expert evaluation into our considerations in designing neural network-based intelligence system. Our goal is aimed at the development of an intelligence system to estimate and track changes in tumors over time during diagnosis and treatment. The precise relationship between tactile quantities and the breast texture and abnormalities is complex. Our approach to this problem is to build on tactile signal processing algorithms developed for robotics applications, which relates measured surface stresses to shapes of contact. To analyze tactile abnormalities with computational intelligence, we have designed neural network bases to accurately estimate and track changes in tumors over time.

The precise relationship between the mounted tactile quantities and the breast texture and abnormalities is complex. Some work has recently appeared on this inversion problem for palpation applications, but the success of this approach is limited because it relies on gross force information rather than the pressure distribution information that will be provided by our tactile array sensors. We have previously developed signal processing algorithms for this purpose, which can be modified to map the sensor measurements to the structure of the breast lump [22,27]. This approach will provide a better understanding of breast palpation and establish a basis for constructing refined palpation devices. Our main contribution in the field of medical image analysis is in the development of vision type neural networks, fractal imaging, contextual segmentation, and advanced pattern recognition techniques.

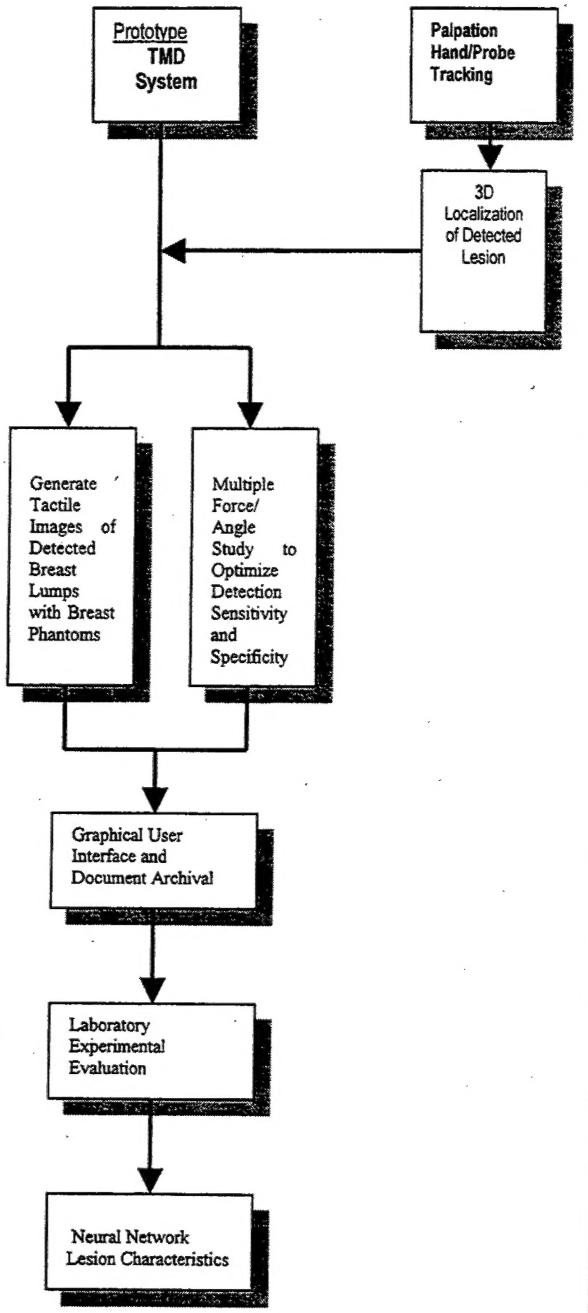

Figure 1. Step in the development of TMD system for breast lump characterization that will demonstrate the feasibility of neural network classifies

We have put considerable effort on the development of the convolution neural network (CNN) and its associated training methods. Figure 3 shows the typical structure of CNN. The structure of the CNN is a simplified version of "neocognitron," which simulates the network structure and signal propagation in vertebrate animals. The structure of the CNN is used as one of the fundamental research tools of the proposed research. We found that the performance of the CNN is more powerful than a regular fully connected neural network, such as the Multilayer perceptron (MLP) neural network, in disease pattern recognition.
The Soft tissue analysis for the characterization of palpable breast lesions requires:

(1) The quantitative measurement of applied forces and tactile images of pressure distribution during palpation,
(2) The construction of the tactile featured database and training algorithms, and
(3) The estimation of key tactile parameter values associated with detected lesions through a neural network based soft tissue modeling and analysis.

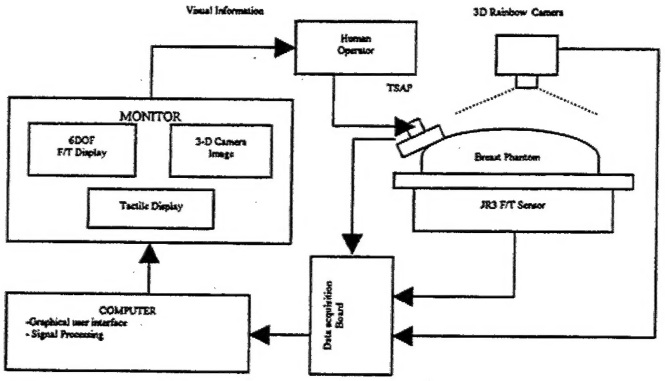

Figure 2. System block diagram of prototype TMD.

During the experiments, the forces/torques applied by the human examiner during the palpation are recorded in terms of six force parameter values: Fx, Fy, Fz, Mx, My, Mz. The TMD is used to acquire various tactile images, by palpating the site after the examiner locates the lesion by initial hand palpation. Since the relationships between the tactile images and lesion characteristics are expected to be complex and nonlinear, we believe that the inverse problem (extraction of lesion characteristics from tactile images) can be solved when sufficient tactile information is acquired. As a result, for each lesion, after pushing the TMD against the breast to achieve certain level of force, the examiner rotates the TMD to five different orientations at each of which the information about the forces/torques and tactile image are simultaneously recorded. OR1 is the initial orientation of the TMD after being pushed by the examiner to a certain level of force. OR2, OR3, OR4 and OR5 are the TMD orientations after it is rotated forward, backward, left and right, respectively. Figure 2. shows the prototype of the tactile mapping system, where an 8x8 tactile sensor array and a 6DOF force/torque sensor is employed. In order to demonstrate the effectiveness of the tactile mapping device for the characterization and documentation of detected lumps, intensive experiments have been conducted to pilot-test the sensitivity and reproducibility of the system in measuring the applied forces and pressure profiles due to lumps. Examining the graphical displays in Figure 5.b and 5.c in comparison with that of the case with no lesions (Figure 5.a), we noticed that a peak consistently occurred in the display. We can draw preliminary conclusions that a peak in the graphical display indicates the existence of a lesion. The output from our TMD will be used as an input for our neural network.

A convolution neural network (CNN) based soft tissue modeling and analysis technique is developed to estimate lesion sizes and depth, shown in Figure 4, where each input denotes a cluster corresponding to the tactile image of one force projection, and each hidden cluster extracts appropriate tactile features to highlight mass characteristics. The CNN outputs consist of two sets of signals: parameter estimates, and reconstructed tactile profiles.

In neural network based mass detection, we collected the output from our TMD used the output as inputs to our neural network. We separated our database into two sets; one set will be used for training, and the remaining set will be used for testing. This database was used to train two neural network systems:

(1) A conventional 3-layer back propagation neural network
(2) A CNN training method

The error back propagation algorithm trained both neural network systems by feeding the features from the input layer, and registering the corresponding target value at the output side. Once the training of the neural networks is complete, we will then use the remaining sets for the testing.

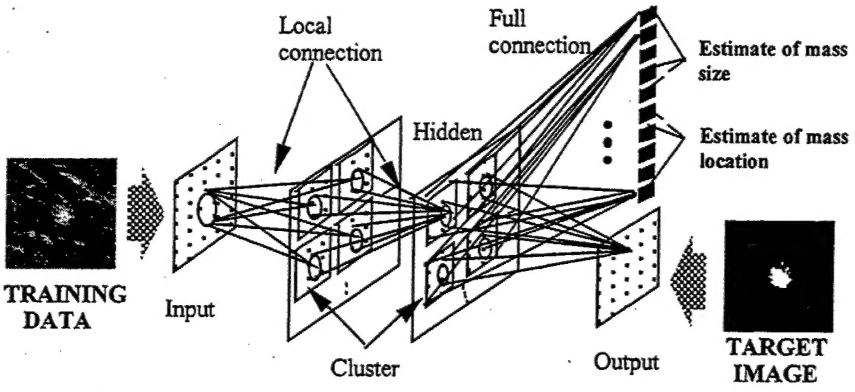

Figure 3. Convolution neural network (CNN) based breast tumor characterization and parameter estimation where the inputs are the tactile images and associated applied angles and forces, and the outputs are the estimated size and depth of the lump and associated probability of being a tumor.

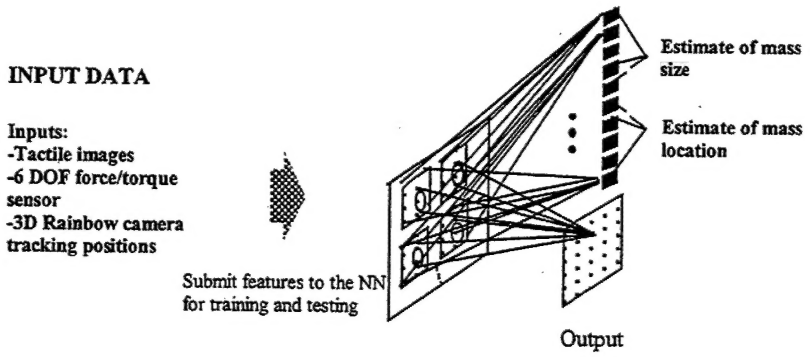

Figure 4. Shows the outputs from our TMD will be used as an input to our convolution neural network based breast tumor characterization and parameter estimation.

We applied several image processing and training methods designed to mimic a physician's interpretation using the breast lump database. The TMD will be evaluated by physicians, and will undergo a limited evaluation of diagnosis and documentation using simulations. Clinical evaluations will be carried out under the supervision of Dr. Matthew Freedman. In particular, we will evaluate the sensitivity, accuracy, and precision of the tactile sensors during simulated CBE applications.

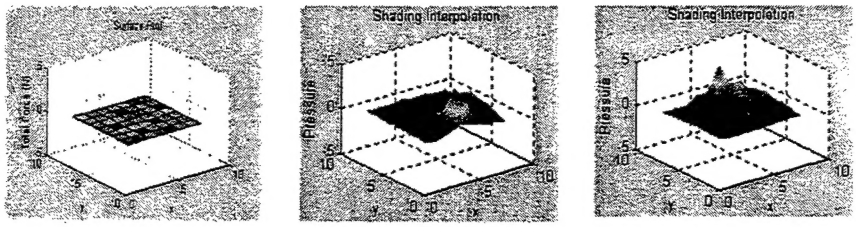

(a) (b) (c)

Figure 5. The graphical displays of tactile sensor.

KEY RESEARCH ACCOMPLISHMENTS:

Our key goal of Task II is to develop a neural network based intelligence system that estimates and tracks the changes (in size and depth) of the tumors over time after diagnosis and during treatment to develop a neural network. Our accomplishments in Task II are the following:

- By taking the feedback from experts, we have evaluated the TMD's performance in improving diagnosis in terms of precision, sensitivity, and specificity. We have re-designed a prototype TMD system based on the feedback from the model-based laboratory evaluations, and preliminary expert evaluations.

- We have designed a suitable neural network-based intelligence system for tactile signal interpretation. By combining the knowledge of vision-based neural networks, tactile sensing technologies are integrated for the investigation of soft tissue interactions with the tactile/force sensor, where hard inclusions (breast lump) can be characterized through neural network learning capabilities

- We have developed neural network training algorithms and computer interpretation codes, convolution neural network (CNN) based breast tumor characterization and parameter estimation; the inputs are the tactile images and associated applied angles and forces; the outputs are the estimated size and depth of the lump and associated probability of being a tumor.

REPORTABLE OUTCOMES:

- R. Srikanchana, K. Huang, J. Xuan, M. Freedman, and Y. Wang, "Mixture of Principal Axes Registration for Change Analysis in Computer-Aided Diagnosis," *30th Applied Imagery Pattern Recognition Workshop*, Washington, DC, October 2001.

- R. Srikanchana, Y. Wang, C. C. Nguyen, and M. Freedman, "Tactile Imaging of Palpable Breast Cancer," *Proc. SPIE Medical Imaging,* vol. 4682, San Diego, CA, February 2002.

- R. Srikanchana, J. Xuan, M. Freedman, and Y. Wang "Mixture of principal axes registration: a neural computation approach," *Proc. SPIE Medical Imaging,* vol. 4684, San Diego, CA, February 2002

- Presented the paper "Mixture of Principal Axes Registration for Change Analysis in Computer-Aided Diagnosis," *30th Applied Imagery Pattern Recognition Workshop*, Washington, DC, October 2001.

- Presented the poster "Tactile Mapping and Tumor Modeling for Breast Cancer Detection," *The third Era of Hope meeting for the Department of Defense (DOD) Breast Cancer Research Program (BCRP)*, Orlando, FL, September 2002.

CONCLUSIONS:

This project is concerned with the detection of lumps in breast palpation using a tactile mapping device (TMD) system. It presented the main components of the TMD and explained their operations. Experiments were conducted on a breast model to detect different types of lumps. Experimental data showed that the peak in the display of pressure distribution of the TMD indicated the presence of a lump. The knowledge of vision-based neural networks and tactile sensing technology are integrated for the first time for investigations of soft tissue interactions with the tactile/force sensor; the hard inclusion (breast cancer) can be characterized through neural network learning capabilities, instead of using a simplified complex biomechanics model with many heuristic assumptions. Tactile mapping systems using convolution neural networks and tactile sensing arrays can extract invariant properties of the detected breast lump, and make it possible for the first time to quantitatively and objectively record the processes and findings of a breast palpation. With the proven power of nonlinear signal processing using both convolution neural networks (CNN) and multi-layer perceptron (MLP), we expect that the tactile parameters associated with the lesions (i.e., the size and depth of the lesion) can be estimated more accurately than those by the conventional approaches using the first principle of engineering.

REFERENCES:

1) American Cancer Society, *Cancer Facts and Figures*, Technical Report, 1994.
2) Rimer BK. Breast Cancer Screening. In Harris JR, Lippman ME, Morrow M, Hellman S. Diseases of the Breast. 1996. Pp 307-322.
3) Geng, J, "Rainbow 3D Camera - A New Concept for High Speed and Low-Cost 3D Vision", *Journal of Optical Engineering* Vol.35, No.2, p376, Feb 1996.
4) Wang Y, Nguyen C, Srikanchana R, Geng J, and Freedman MT, "Tactile mapping of palpable abnormalities for breast cancer diagnosis," *Proc. IEEE Conf. Robotics and Automation*, Detroit, 1999.
5) R. Srikachana, Y. Wang, C. Nguyen, and M. T. Freedman, "Soft Tissue Modeling in Palpable Lesion Characterization by Tactile Mapping Neural Networks," to appear *Proc. Intl. Joint Congress Neural Nets*, 1999.
6) Zeng J, Wang Y, Freedman MT, and Mun SK, "Finger tracking for breast palpation quantification using color image features," *Journal of Optical Engineering*, 36(12): 3455-3461, December 1997.
7) Dario, P and Bergamasco, M, "An advanced robot system for automated diagnosis tasks through palpation," *IEEE Trans. Biomed. Eng.*, vol. 35, no. 2, pp.118-126, February 1988.
8) Fearing, RS, "Tactile sensing mechanisms," *Intl. J. Robotics Research*, 9(3): 3-23, 1990.
9) Fletcher SW, O'Malley MS, and Bunce LA, "Physician's abilities to detect lumps in silicone breast models," *JAMA*, 253(15):2224-2228, 1985.
10) Howe, RD, Peine WJ, Kontarinis, DA, Son, J, "Remote palpation technology," *IEEE Engineering in Medicine and Biology*, 14(3): 318-323, May/June 1995.
11) Wellman, PS, "A biomechanical model for tactile mapping of palpable abnormalities," Harvard Robotics Lab Technical Report 96-002, Harvard University, 1996.
12) Foster RS, Worden JK, Costanza MC, and Solomon LJ, " Clinical breast examination and breast self-examination: past and present effect on breast cancer survival," *Cancer*, 69(7): 1992-1998, 1992.
13) American Cancer Society Brochure F-362, *How to Examine Your Breasts*, 1994.
14) J. Ophir, I. Cespedes, H. Ponnekanti, Y. Yazdi, and X. Li, "Elastography: a quantitative method for imaging the elasticity of biological tissues," *Ultrasonic Imaging*, 13:111-134, 1991.
15) C. D. Haagensen, *Physicians' Role in the Detection and Diagnosis of Breast Disease: Palpation of the Breast, Diseases of The Breast*, 3rd ed. Philadelphia: Saunders, pp.521-527, 1986.
16) H. S. Bloom et als., "Major stimulus dimensions determining detection of simulated breast lesions," *Perception and Psychophysics*, Vol. 32, pp. 251-260, 1982.
17) D. C. Hall, C. K. Adams, G. H. Stein, H. S. Stephenson, M. K. Goldstein, and H. S. Pennypacker, "Improved Detection of Human Breast Lesions," *Cancer*, Vol. 46, pp. 400-413, July 1980.
18) B. P. Haughey, J. R. Marshall, C. Mettlin, T. Nemoto, K. Kroldart, and M. Swanson, "Nurse's Ability to Detect Nodules in Silicone Breast Models," *Oncology Nursing Forum*, Vol. 11, No. 1, pp. 37-42, 1984.
19) M. S. O'Malley and S. W. Fletcher, "Screening for Breast Cancer With Breast Self-Examination A Critical Review," *JAMA*, Vol. 257, No. 16, pp. 2197-2203, 1987.
20) R. D. Howe, "Touch sensing and display for surgical applications," robotics, Vol. 4, No. 1, 1995.
21) R. D. Howe et als., "A tactile sensing and display system for teleoperated manipulation," *Proc. IEEE Intl. Conf. Robotics Auto.*, pp. 641-646, Nagoya, Japan, May 1995.
22) R. S. Fearing and J. M. Hollerbach, "Basic solid mechanics for tactile sensing," *Intl. J. Robotics Research*, 4(3): 40-54, Fall 1985.
23) J. M. Rehg and T. Kanade, "Visual tracking of high DOF articulated structures: an application to human hand tracking," *Proc. 3th European Conf. Computer Vision*, 1994.

24) T. Darrell and A. Pentland, "Space-time gestures," *Proc. IEEE Conf. Computer Vision and Pattern Recognition*, 1993.
25) N. A. Langrana, G. Burdea, M. Dinsmore, D. Gomez, E. Harper, D. Silver, and N. Mezrich, "Virtual reality training simulation with force feedback: palpation of lesions," *Private communications* with Dr. Joseph Wang and Dr. Matthew Freedman, 1996-present.
26) E. J. Nicolson, "Tactile sensing and control of a planar manipulator," Ph.D. Thesis, University of California Berkeley, 1994.
27) E. J. Nicolson and R. S. Fearing, "The reliability of curvature estimates from linear elastic tactile sensors," *Proc. IEEE Intl. Conf. Robotics Auto.*, Nagoya, Japan, May 1995.
28) R. D. Howe and M. R. Kutkosky, "Dynamic tactile sensing: perception of fine surface features with stress rate sensing," *IEEE Trans. Robotics & Auto.*, 9(2):140-151, April 1993.
29) Pennypacker HS, *Private Communications* with Dr. Joseph Wang, 1996-present.
30) R. S. Fearing and T. O. Binford, "Using a Cylindrical Tactile Sensor for Determining Curvature," *IEEE Trans. Robotics and Automation,* December 1991.
31) B. Gray and R. S. Fearing, "A Surface-Micromachined Microtactile Sensor Array," *IEEE ICRA*, Minneapolis, April 1996.
32) W. J. Peine and R. D. Howe, "Finger Pad Shape in Lump Detection," *ASME Summer Bioeng. Conf.,* Sun River Oregon, June 1997.
33) P. S. Wellman and R. D. Howe, "Modeling Probe and Tissue Interaction for Tumor Feature Extraction," *ASME Summer Bioeng. Conf.,* Sun River Oregon, June 1997.

APPENDICES:

R. Srikanchana, K. Huang, J. Xuan, M. Freedman, and Y. Wang, "Mixture of Principal Axes Registration for Change Analysis in Computer-Aided Diagnosis," *30th Applied Imagery Pattern Recognition Workshop*, Washington, DC, October 2001.

R. Srikanchana, Y. Wang, C. C. Nguyen, and M. Freedman, "Tactile Imaging of Palpable Breast Cancer," *Proc. SPIE Medical Imaging,* vol. 4682, San Diego, CA, February 2002.

R. Srikanchana, J. Xuan, M. Freedman, and Y. Wang "Mixture of principal axes registration: a neural computation approach," *Proc. SPIE Medical Imaging,* vol. 4684, San Diego, CA, February 2002

30th Applied Imagery Pattern Recognition Workshop
Washington, DC
Oct. 2001

Mixture of Principal Axes Registration for Change Analysis in Computer-Aided Diagnosis

Rujirutana Srikanchana[1], Kun Huang[1], Jianhua Xuan[1], Matthew Freedman[2], and Yue Wang[1]
[1]Department of EE/CS, The Catholic University of America
[2]Department of Radiology, Georgetown University Medical Center

Abstract

Non-rigid image registration is a prerequisite for many medical image analysis applications such as image fusion of multi-modality images and quantitative change analysis of a temporal sequence in computer-aided diagnosis. By establishing the point correspondence of the extracted feature points, it is possible to recover the deformation using nonlinear interpolation methods such as the thin-plate-spline approach. However, it is a difficulty task to establish exact point correspondence due to the high complexity of nonlinear deformation existed in medical images. In this paper, a mixture of principal axes registration (mPAR) method is proposed to resolve the correspondence problem through a neural computational approach. The novel feature of mPAR is to align two point sets without needing to establish explicit point correspondence. Instead, it aligns the two point sets by minimizing the relative entropy between their probability distributions resulting in a maximum likelihood estimate of the transformation matrix. The registration process consists of: (1) a finite mixture scheme to establish an improved point correspondence and (2) a multilayer perceptron neural network (MLP) to recover the nonlinear deformation. The neural computation for registration used a committee machine to obtain a mixture of piece-wise rigid registrations, which gives a reliable point correspondence using multiple extracted objects in a finite mixture scheme. Then the MLP is used to determine the coefficients of a polynomial transform using extracted cross points of elongated structures as control points. We have applied our mPAR method to a temporal sequence of mammograms of a single patient. The experimental results show that mPAR not only improves the accuracy of the point correspondence but also results in a desirable error-resilience property for control point selection errors.

1 Introduction

Image registration is an essential step for many medical image analysis applications such as image fusion of multimodality images and quantitative change analysis of a temporal sequence in computer-aided diagnosis. Due to complicated by misregistrations caused by patient motion and physical change, the estimation of transformational geometry from two point sets is an essential step to medical image fusion and computer vision [1, 2]. The task is to recover a matrix representation requiring a set of correspondence matches between features in the two coordinate system [3]. Assume two 3-D data point sets $\{\mathbf{p}_{iA}\}$ and $\{\mathbf{p}_{iB}\}$; $i = 1, 2, ..., N$ are related by

$$\mathbf{p}_{iB} = \mathbf{R}\mathbf{p}_{iA} + \mathbf{T} + \mathbf{N}_i \quad (1)$$

where $\mathbf{R}$ is a rotation matrix, $\mathbf{T}$ is a translation vector, and $\mathbf{N}_i$ is a noise vector. Given $\{\mathbf{p}_{iA}\}$ and $\{\mathbf{p}_{iB}\}$, Arun *et. al* present an algorithm for finding the least-squares solution of $\mathbf{R}$ and $\mathbf{T}$, which is based on the decoupling translation and rotation and the singular value decomposition (SVD) of a 3×3 cross-covariance matrix [3].

The major limitation of the present method is twofold: (1) while feature matching methods can give quite accurate solutions, obtaining correct correspondences of features is a hard problem, especially in the cases of images acquired using different modalities or from inter-subjects; and (2) a rigidity assumption is heuristically imposed while those newly developed deformable matching methods can be computationally expensive and typically need good initial guesses to assure correct convergence [2, 4]. One popular method that is correspondenceless is the principal axes registration (PAR) [1], that is based on the relatively stable geometric properties of image features, i.e., the geometric information contained in these stable image features is often sufficient to determine the transformation between images [2]. Once again, it cannot handle the cases with non-rigid objects.

We present a neural computation based non-rigid registration using piece-wise rigid transformation. The novel

feature is to align two point sets without needing to establish explicit point correspondences, where the derivation is realized by minimizing the relative entropy between the two point distributions resulting in a maximum likelihood estimate of the transformation matrix. That is rather than using a single transformation matrix which give a large registration error, we attempt to interpolatively apply a mixture of transformations. By further generalizing PAR to a mixture of principal axes registration (mPAR) scheme, with soft partitioning of the data set, the mixture is fit using expectation-maximization algorithm, to estimate the transformational of the orthogonal set of eigenvalues and eigenvectors of the auto-covariance matrix. By applying a committee machine to a non-rigid registration, we can acquired the registration based on a mixture of piece-wise transformations of the data set. Then the correspondences control points are obtained. As a final step, the warped image is obtaining using the neural network based non-linear mapping, to obtain the polynomial transform based on extracted control points using multilayer perceptron neural network.

2 Method

Suggested by information theory [5], we note that, since the control point sets in two images can be considered as two separate realizations of the same random source, we do not need to establish point correspondences to extract the transformation matrix. In other words, if we denote by $P_{\{\mathbf{p}_i\}}$ the distribution of the control point set in an image, we have the simple relationship

$$P_{\{\mathbf{p}_{jB}\}} = P_{\{\mathbf{R}\mathbf{p}_{iA}+\mathbf{T}\}} + \epsilon \qquad (2)$$

where ϵ is the noise component. Since the probability distributions can be computed independently on each image without any need to establish feature correspondences, and given the two distributions of the control point sets in the two images, we can recover the transformation matrix in a simple fashion [2].In order to establish feature correspondence between the two images, we applied our segmentation method to extract the control points between two images. After the control has been established, we applied our registration method to the images, as we now sketch.

2.1 Control Point Extraction

Assume that each pixel in the MR image can be decomposed into pixel images x and context image l. By ignoring information regarding the spatial ordering of pixels, we can treat context images as random variables and describe them using a multinomial distribution with unknown parameters π_k, $k = 1, ..., K$, which can be interpreted as a prior probability of pixel labels determined by the global context information. In particular, based on the statistical properties of MR pixel images, where pixel image is defined as the observed gray level associated with the pixel, use of Standard Finite Normal Mixture (SFNM) distribution is justified to model the image histogram by determining the optimal parameters with respect to a distance measure of a sum of the following general form:

$$f_r(x) = \sum_{k=1}^{K} \pi_k g(x|\mu_k, \sigma_k^2)$$

with $\sum_{k=1}^{K} \pi_k = 1, \pi_k \geq 0$, and

$$g(x|\mu_k, \sigma_k^2) = \frac{1}{\sqrt{2\pi}\sigma_k} \exp(-\frac{(x-\mu_k)^2}{2\sigma_k^2})$$

where μ_k and σ_k are the mean and variance of the kth Gaussian kernel, and π_k is the global regularization parameter. We use K to denote the number of Gaussian components and r to denote the parameter vector. This tissue quantification is achieved through three completely unsupervised steps: (1) parameter initialization by optimal histogram quantization; (2) model estimation by histogram based fast expectation-maximization (EM) algorithm; and (3) model selection by minimum description length (MDL) criterion. It is shown that the SFNM model converges to the true distribution when the pixel image are asymptotically independent [18].

After we obtain the optimal parameters for all components, we use a multiple thresholding procedure for initializing image segmentation based on maximum likelihood (ML) principle, which is followed by contextual Bayes relaxation labeling (CBRL) algorithm to obtain a consistent labeling solution based on localized SFNM formulation for improving initial segmentation by using neighborhood text regularities.

We define the component in localized SFNM by the support function:

$$S_i(k) = \pi_k^{(i)} \frac{1}{\sqrt{2\pi}\sigma_k} \exp(-\frac{(x-\mu_k)^2}{2\sigma_k^2})$$

where $\pi_k^{(i)}$ is the local conditional prior of regions, the support function $S_i(k)$ is a function of the component (tissue type) k. Then tissue segmentation is interpreted as the satisfaction of a system of inequalities as follows:

$$S_i(l_i) \geq S_i(k)$$

for all k and for $i = 1, ..., N$, where $l_i, i = 1, ..., N$ is the context images, and a consistent labeling is defined as the one having maximum support at each pixel simultaneously. We further define the average local consistency measure:

$$A(l) = \sum_{i=1}^{N} \sum_{k} I(l_i, k) S_i(k)$$

to link consistent labeling to global optimization[19].

2.2 Registration

For observation of the distributions, we can estimate $\mathbf{R}$ and $\mathbf{T}$ by minimizing the relative entropy (Kullback-Leibler distance) between $P_{\{\mathbf{p}_{jB}\}}$ and $P_{\{\mathbf{R}\mathbf{p}_{iA}+\mathbf{T}\}}$. The least relative entropy estimator is then defined as

$$\arg\min_{\mathbf{R},\mathbf{T}} D(P_{\{\mathbf{p}_{jB}\}} || P_{\{\mathbf{R}\mathbf{p}_{iA}+\mathbf{T}\}}) \tag{3}$$

where D denotes the relative entropy measure. Following the same strategy to decoupling translation and rotation as in [3], we can define a new data point by $\mathbf{q}_{iA} = \mathbf{p}_{iA} - \mathbf{p}_A^0$ and $\mathbf{q}_{jB} = \mathbf{p}_{jB} - \mathbf{p}_B^0$, where $\mathbf{p}_A^0$ and $\mathbf{p}_B^0$ are the centroids of $\{\mathbf{p}_{iA}\}$ and $\{\mathbf{p}_{jB}\}$ respectively. Then the optimal geometric transformations, $\mathbf{R}$ and $\mathbf{T}$, are defined as

$$\mathbf{R} = \mathbf{U}_B \mathbf{H} \mathbf{U}_A^t \text{ and } \mathbf{T} = \mathbf{p}_B^0 - \mathbf{R}\mathbf{p}_A^0 \tag{4}$$

where the superscript t denotes matrix transposition, $\mathbf{U}_A$ and $\mathbf{U}_B$ are 3×3 orthonormal matrices, and $\mathbf{H}$ is a 3×3 diagonal matrix with element $h_m = \sqrt{\lambda_{mB}/\lambda_{mA}}$. Note that the transformation $\mathbf{U}$ consists of the orthonormal set of eigenvectors and h_m is the squared root of the eigenvalues λ_m of the auto-covariance matrix $\mathbf{C}$ for $m = 1, 2, 3$ and for $\{\mathbf{p}_{iA}\}$ and $\{\mathbf{p}_{jB}\}$, respectively.

However, because of its global linearity, the application of PAR is necessarily somewhat limited [6]. An alternative paradigm is to model a multimodal control point set with a collection of local linear models. The method is a two-stage procedure: a soft partitioning of the data set followed by estimation of the principal axes within each partition [7]. Recently there has been considerable success in using standard finite normal mixture (SFNM) to model the distribution of a multimodal data set and the association of a SFNM distribution with PAR offers the possibility of being able to register two images through a mixture of probabilistic principal axes transformations [7]. Assume that there are K_0 control point clusters, where each control point cluster defines a transformation $\{\mathbf{R}_k, \mathbf{T}_k\}$. Thus for a point $\mathbf{p}_{nA}$, its new locations corresponding to each of the transformations are $\mathbf{p}_{nk} = \mathbf{R}_k \mathbf{p}_{nA} + \mathbf{T}_k$ for $k = 1, ..., K_0$. Further assume that the control point set defines a SFNM distribution

$$f(\mathbf{p}_i) = \sum_{k=1}^{K_0} \pi_k g(\mathbf{p}_i | \mu_k, \mathbf{C}_k) \tag{5}$$

where g is the Gaussian kernel with mean vector μ_k and auto-covariance matrix $\mathbf{C}_k$, and π_k is the mixing factor proportional to the number of control points in cluster k. For each of the control point sets $\{\mathbf{p}_{iA}\}$ and $\{\mathbf{p}_{iB}\}$, the mixture is fit using the expectation-maximization (EM) algorithm. The E step involves assigning to the linear models responsibilities from the control points; the M step involves re-estimating the parameters of the linear models in the light of this assignment [7].

Thus the statistical membership of point $\mathbf{p}_{nA}$ belonging to each of the control point clusters can be derived by

$$z_{nk} = P(\mathbf{R}_k, \mathbf{T}_k | \mathbf{p}_{nA}) = \frac{\pi_{kA} g(\mathbf{p}_{nA} | \mu_{kA}, \mathbf{C}_{kA})}{f(\mathbf{p}_{nA})} \tag{6}$$

i.e., the posterior probability of $\{\mathbf{R}_k, \mathbf{T}_k\}$ given $\mathbf{p}_{nA}$. Thus, we can define the FMR transformation as

$$\mathbf{p}_n = \sum_{k=1}^{K_0} z_{nk} \mathbf{p}_{nk} = \sum_{k=1}^{K_0} \frac{\pi_{kA} g(\mathbf{p}_{nA} | \mu_{kA}, \mathbf{C}_{kA})}{f(\mathbf{p}_{nA})} (\mathbf{R}_k \mathbf{p}_{nA} + \mathbf{T}_k) \tag{7}$$

where $\{\mathbf{R}_k, \mathbf{T}_k\}$ is determined based on $f(\mathbf{p}_i) = \sum_{k=1}^{K_0} \pi_k g(\mathbf{p}_i | \mu_k, \mathbf{C}_k)$ that we have estimated in the previous step using the EM algorithm. Note that now we do need the correspondences between the two control point clusters, and these correspondences may be found, after a global PAR is initially performed, by using a site model supported approach or a dual-step EM algorithm to unify the tasks of estimating transformation geometry and identifying cluster-correspondence matches [4]. This philosophy for recovering transformational geometry of the non-rigid objects is similar in spirit to the *divide-and-conquer* principle [6], under which the relative entropy between the two point sets reaches its minimum

$$\arg\min_{\mathbf{R}_k, \mathbf{T}_k} D(P_{\{\mathbf{p}_{jB}\}} || P_{\{\sum_{k=1}^{K_0} z_{ik}(\mathbf{R}_k \mathbf{p}_{iA} + \mathbf{T}_k)\}}) \tag{8}$$

both globally and locally.

Based on a mixture of probabilistic principal axes transformations, the next section describes a neural computation using a committee machine approach for which a complex computational task is solved by dividing it into a number of computationally simple tasks and then combining the solutions to those tasks.

2.2.1 Neural Computation

A neural network interpretation of the EM algorithm is given in [8]. Because of its reputation of being slow in which new information acquired in the expectation step is not used immediately, on-line versions of the EM algorithm are proposed for large-scale sequential learning. Thus, we adopt a fully unsupervised and incremental stochastic learning algorithm. The scheme provides winner-takes-in probability (Bayesian "soft") splits of the control points, hence allowing the data to contribute simultaneously to multiple clusters which results in

$E-Step$

$$z_{(i+1)k} = \frac{\pi_k^{(i)} g(\mathbf{p}_{i+1}|\mu_k^{(i)}, \mathbf{C}_k^{(i)})}{f(\mathbf{p}_{i+1}|\pi_k^{(i)}, \mu_k^{(i)}, \mathbf{C}_k^{(i)})} \quad (9)$$

$M-Step$

$$\mu_k^{(i+1)} = \mu_k^{(i)} + a(i)(\mathbf{p}_{i+1} - \mu_k^{(i)}) z_{(i+1)k}, \quad (10)$$

$$\mathbf{C}_k^{(i+1)} = \mathbf{C}_k^{(i)} + b(i)[(\mathbf{p}_{i+1} - \mu_k^{(i)})(\mathbf{p}_{i+1} - \mu_k^{(i)})^T - \mathbf{C}_k^{(i)}] z_{(i+1)k}, \quad (11)$$

$$\pi_k^{(i+1)} = \frac{i}{i+1}\pi_k^{(i)} + \frac{1}{i+1} z_{(i+1)k} \quad (12)$$

for $k = 1, ..., K_0$ and for $\{\mathbf{p}_{iA}\}$ and $\{\mathbf{p}_{iB}\}$, respectively, where $a(i)$ and $b(i)$ are introduced as the learning rates, two sequences converging to zero, ensuring unbiased estimates after convergence. This procedure is termed as neural computation of the EM algorithm, where at each complete cycle of the algorithm, we first use "*old*" set of parameter values to determine the posterior probabilities $z_{(i+1)k}$. These posterior probabilities are then used to obtain "*new*" values $\pi_k^{(i+1)}, \mu_k^{(i+1)}, \mathbf{C}_k^{(i+1)}$. The algorithm cycles back and forth until the value of relative entropy between the data histogram and mixture model reaches its minimum

$$\arg \min_{\pi_k, \mu_k, \mathbf{C}_k} D(P_{\{\mathbf{p}_i\}} || f(\mathbf{p}_i)) \quad (13)$$

for $\{\mathbf{p}_{iA}\}$ and $\{\mathbf{p}_{iB}\}$, respectively.

With a soft partitioning of the data set using Eqs. (9-12), control points will now effectively belong to more than one cluster spatially. Thus, the effective input values are $\mathbf{p}_{ik} = z_{ik}(\mathbf{p}_i - \mu_k)$ for an independent registration transformation k in the committee machine [9]. We then extend our adaptive principal components extraction (APEX) algorithm to a probabilistic version, i.e., PAPEX [10], to determine $\mathbf{U}_k$ for $\{\mathbf{p}_{iA}\}$ and $\{\mathbf{p}_{iB}\}$, respectively.

Consider the modular network nature of Eq. (7), it is a mixture of local expert model, in which the individual responses of the experts are nonlinearly combined by means of a single gating network. It is assume here that the different experts work best in different regions of the input space in accordance with the probabilistic generative model. In our case, the effective input values are $\mathbf{p}_{ik} = z_{ik}(\mathbf{p}_i - \mu_k)$ for an independent registration transformation k in the networks. A committee machine consists of k supervised modules, with a soft partitioning of the data set using EM algorithm called experts, and an integrating unit called a gating network that performs the function PAPEX to determine the transformation of the orthogonal set of eigenvalues and eigenvectors of the auto-covariance matrix among the expert networks. The output of our committee machine is a transformational matrix of image pair. Based on those correspondences between the two images, the control points

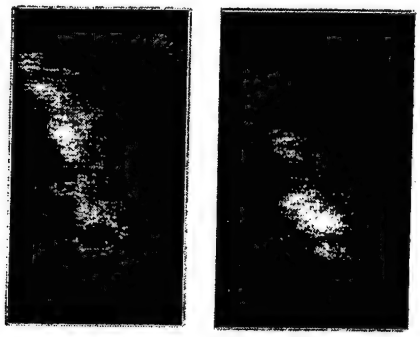

Figure 1. A pair of real mammograms taken over a period of time from the same patient.

are obtained. The final step is to calculate the polynomial transformation using piece-wise interpolation. In our case for a given corresponding control points pair of the image, we considered neural network based MLP to recover the nonlinear deformation. The final result shows the warped image that has been corrected by applied our neural computation to correct most of the scale different between the images.

3 Results and Discussion

We applied our algorithm to a temporal sequence of mammograms of a single patient [15]. In this example, the committee machine is used to obtain an initial registration using multiple extracted objects (skinline, dense tissue regions) in a finite mixture scheme. Then MLP was used to determine the coefficients of a polynomial transform using extracted vertical and horizontal cross points of elongated structures as control points. Previously, thin-plate spline (TPS) was used to determine the transform coefficients [13]. As a comparison, we consider both results here. Figure 1 shows the raw sequence and Figure 2 shows the resulting warped image for MLP (left) and TPS (right). Using image difference (Figure 3) we see that the most of the scale different between images has been corrected by using MLP. While the TPS distorts the image, this distortion can be attributed to control point selection and correspondence. The MLP better adapts to the error present in the control points thus yielding a smoother result.

We applied our approach for the non-rigid registration of contrast-enhanced breast MRI. A 3D breast MRI scan is acquired prior to the injection of contrast agent, followed by a sequence of 3D breast MRI scans after the agent has been applied. The goal of image registration in contrast-enhanced breast MRI is to relate any point in the post-contrast enhanced sequence to the pre-contrast enhanced

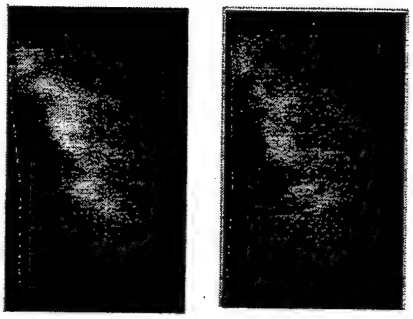

Figure 2. The result of warped current image to previous image (left: MLP; right: TPS).

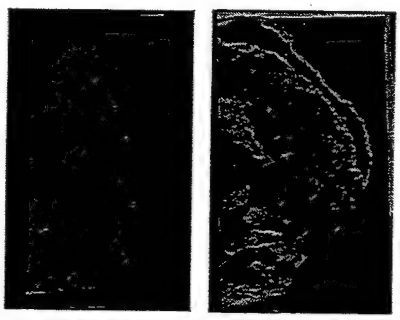

Figure 3. Image difference (left: MLP; right: TPS)

Figure 4. Segmentation of Fibro-Tissue

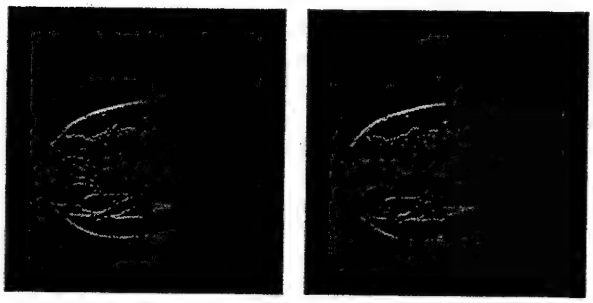

Figure 5. A pair of a contrast-enhanced in MRI (Left: pre-contrast image; right: post-contrast image.)

reference image. After we performed a pre-registration using PAR method to correct the global alignment between images, we applied our segmentation algorithm to extract the control objects between two images. Figure 4 shows the segmentation of Fibro-tissue. Next, we applied the proposed non-rigid registration to these images using the control objects that has been acquired by the segmentation. Figure 5 shows a pre- and post-contrast enhanced image of the patient data set with a propose registration method. Figure 6 shows the post-contrast enhanced image and corresponding difference images after registration. The results demonstrate that the simple image differencing can isolate such area.

4 Conclusions

In this paper, we presented the theoretical concepts and methods of a neural computation based non-rigid registration algorithm for computer-aided diagnosis. The approach uses a committee machine to recover the total transformational geometry of the non-rigid object using multiple rigid transforms combined together in a mixture of principal axes registration scheme. Finite mixture transform combination is a novel technique to combine multiple transforms that are contained in a single image. Other than local transforms no other method combines multiple transforms together. In ad-

Figure 6. Difference image to highlight enhanced area.

dition finite mixture combinations, yields a smooth image while local transforms yield an image containing discontinues on transform boundaries. In addition, the registration obtained in the committee machine is fine tuned using a non-linear transform generated by a MLP network using extracted control points.

We applied our non-rigid algorithm to a temporal sequence of breast image of a single patient. Some distortion can be seen in the final warped images because of the error in control point selection and correspondence. Improvement is this portion should decrease distortion and yield a smoother looking image. Using neural networks in this problem has increased the generality of this approach by allowing the algorithm to adjust performance as imaging condition change.

5 Acknowledgments

This research was supported by the Department of Defense under Grant DAMD17-98-8045 and DAMD17-00-0195. The authors would like to thank the experts whose name are presented in our early papers for their valuable time and great assistance.

References

[1] M. Moshfeghi and H. Rusinek, "Three-dimensional registration of multimodality medical images using the principal axes techniques," *Philips J. Res.*, vol. 47, no.2, pp. 81-97, 1992.

[2] V. Govindu and C. Shekhar, "Alignment using distributions of local geometric properties," *IEEE Trans. Pattern Anal. Machine Intell.*, vol. 21, no.10, pp. 1031-1043, October 1999.

[3] K. S. Arun, T. S. Huang, and S. D. Blostein, "Least-Squares Fitting of Two 3-D Point Sets," *IEEE Trans. Pattern Anal. Machine Intell.*, vol. 9, no.5, pp. 698-700, September 1987.

[4] A. D.J. Cross and E. R. Hancock, "Graph matching with a dual-step EM algorithm," *IEEE Trans. Pattern Anal. Machine Intell.*, vol. 20, no.11, pp. 1236-1253, November 1998.

[5] T. M. Cover and J. A. Thomas, *Elements of Information Theory*, New York: Wiley, 1991.

[6] G. E. Hinton, P. Dayan, and M. Revow, "Modeling the manifolds of images of handwritten digits," *IEEE Trans. Neural Nets*, vol. 8, no.1, pp. 65-74, January 1997.

[7] Y. Wang, L. Luo, M. T. Freedman, and S. Y. Kung, "Probabilistic principal component subspaces: A hierarchical finite mixture model for data visualization," *IEEE Trans. Neural Nets*, vol. 11, no. 3, pp. 625-636, May 2000.

[8] L. Perlovsky and M. McManus, "Maximum likelihood neural networks for sensor fusion and adaptive classification," *Neural Networks*, vol. 4, pp. 89-102, 1991.

[9] S. Haykin, *Neural Networks: A Comprehensive Foundation,* 2nd ed., Prentice-Hall, Inc., Upper Saddle River, Ney Jersey, 1999.

[10] S. Y. Kung, *Principal Component Neural Networks*, New York: Wiley, 1996.

[11] M. I. Jordan and R. A. Jacobs, "Hierarchical mixture of experts and the EM algorithm," *Neural Computation,* vol. 6, pp. 181-214, 1994.

[12] D. M. Titterington, A. F. M. Smith, and U. E. Markov, *Statistical analysis of finite mixture distributions*. New York: John Wiley, 1985.

[13] K. Woods, et. al., "Patient Site Model Supported Change Detection," *Proceedings of SPIE Medical Imaging: 2000*, vol.1, no. 24 , pp. 1095-1106, 2000.

[14] J. Lu, R. Srikanchana, M. McClain, Y. Wang, J. Xuan, I. A. Sesterhenn, M. T. Freedman, and S. K. Mun "A Statistical Volumetric Model for Characterization and Visualization of Prostate Cancer," *Proc. SPIE Medical Imaging,* vol. 3976, pp. 142-153, 2000.

[15] K. Woods, *Image Guided Diagnosis through Change Detection in Image Sequences,* Doctoral Dissertation, The Catholic University of America, 2000.

[16] R. Srikanchana, K. Woods, J. Xuan, C. Nguyen, and Y. Wang "Non-Rigid Image Registration by Neural Computations," *Proc. IEEE Neural Networks for Signal Processing,* pp. 413-422, 2001.

[17] P. Santago and H.D. Gage, "Quantification of MR Brain images by mixture density and partial volume modeling," IEEE Trans. Med. Imag., Vol. 12, No. 3, pp. 566-574, Sept. 1993.

[18] Y.Wang and T. Adali,"Efficient learning of finite normal mixtures for image quantification," in Proc. IEEE Int. Conf. Acoustic, Speech, and Signal Processing, Atlanta, GA, 1996, pp. 3422-3425.

[19] R. A. Hummel and S. W. Zucker, "On the foundations of relaxation labeling processes," IEEE Trans. Pattern Anal. Machine Intell., Vol. 5, May 1983.

Tactile Imaging of Palpable Breast Cancer

Rujirutana Srikanchana[a], Yue Wang[a], Matthew Freedman[b], and Charles C. Nguyen[a]

[a]Department of Electrical Engineering and Computer Science,
The Catholic University of America, Washington, DC 20064, USA
[b]Department of Radiology,
Georgetown University Medical Center, Washington, DC 20007, USA

ABSTRACT

This paper presents the development of a prototype Tactile Mapping Device (TMD) system comprised mainly of a tactile sensor array probe (TSAP), a 3-D camera, and a force/torque sensor, which can provide the means to produce tactile maps of the breast lumps during a breast palpation. Focusing on the key tactile topology features for breast palpation such as spatial location, size/shape of the detected lesion, and the force levels used to demonstrate the palpable abnormalities, these maps can record the results of clinical breast examination with a set of pressure distribution profiles and force sensor measurements due to detected lesion. By combining the knowledge of vision based, neural networks and tactile sensing technology; the TMD is integrated for the investigation of soft tissue interaction with tactile/force sensor, where the hard inclusion (breast cancer) can be characterized through neural network learning capability, instead of using simplified complex biomechanics model with many heuristic assumptions. These maps will serve as an objective documentation of palpable lesions for future comparative examinations. Preliminary results of simulated experiments and limited pre-clinical evaluations of the TMD prototype have tested this hypothesis and provided solid promising data showing the feasibility of the TMD in real clinical applications.

Keywords: T actile Mapping Device, Tactile Sensor Array Probe, force/torque sensor, breast palpation, breast cancer, tactile imaging.

1. INTRODUCTION

Physical breast examination is an effective and completely non-invasive method for the detection of breast cancer.[1,3] With a lump as the most common symptom of breast cancer, studies show that the majority of breast cancers was found by palpation which complements mammography, since palpation can evaluate breast tissue near the chest wall and axilia that is not accessible to mammography.[3] In addition, studies have found that as many as 12-15% of cancers that were detected by physical examination were not apparent on mammograms.[1,3]

Unfortunately, breast palpation has been hampered by problems inherent in its subjective nature, leading to difficulty in interpreting and documenting the examiner's impressions of the perceived lump in terms of tumor characteristics.[3] For example, a physician may determine that a palpable suspicious abnormality needs continued monitoring. This requires maintaining a record of the examination results, which at present is limited to verbal notes about parameters such as the position, size, and hardness of the lump. Because it is difficult to verbalize tactile sensations, the subjective and arbitrary nature of these notes makes effective follow-up exams problematic.

We have conducted a study to advance fundamental understanding of palpation and solve these practical problems through the creation of a new tactile mapping device (TMD). This device will measure three key variables during palpation: the examiner's search patterns, the applied forces, and the small-scale pressure variations at the skin due to lumps. We have integrated and pilot-tested a prototype TMD consisting of a

Further author information: (Send correspondence to Rujirutana Srikanchana)
E-mail: 55srikanchan@cua.edu, Telephone: 1 202 319 5243
Address: The Catholic University of America, EE/CS Department, 620 Michigan Ave., Washington, DC, 20064, U.S.A.

Medical Imaging 2002: Physics of Medical Imaging, Larry E. Antonuk, Martin J. Yaffe, Editors,
Proceedings of SPIE Vol. 4682 (2002) © 2002 SPIE ·1605-7422/02/$15.00

novel three-dimensional (3-D) camera that can track finger motion and breast deformation in video speed, a six degree-of-freedom (DOF) force/torque sensing device measuring the applied forces, and a novel pressure distribution sensor array that can image tactile profile of lumps.[1] The primary objective aims that (1) new tactile mapping technology can quantitatively measure the location and applied forces in breast palpation, and the tactile features of detected breast lumps; and (2) new device can accurately characterize and document breast lumps and will improve clinicians' ability to monitor changes in lump across time and possibly to distinguish malignant from benign lumps. From a set of "images" of the suspect mass, a neural network supported pattern analysis system will extract the invariant properties of the lump, such as the depth and size, based on a nonlinear model of sensor-tissue interaction with hard inclusions. This TMD system will make it possible for the first time to quantitatively and objectively record and characterize the processes and findings of breast palpation. While initially the system will be used to perform clinical breast examination, we believe that eventually it may be used in breast self-examination by women through tele-home care.[4,5]

2. SYSTEM OVERVIEW

The goal of this research is to extend the range and resolution of breast palpation methods, thus increasing palpation sensitivity and specificity (i.e, the ability to detect lumps and distinguish clinically significant changes). Using 3-D camera, force sensor, and tactile arrays, we can create reproducible tactile maps (or images) of the palpable abnormalities of the breast. The novel 3-D camera is able to provide real-time 3-D motion measurement (for tactile probe) and surface profile measurement (for breast tissue deformation) at a rate of 30 frames per second. We have further integrated and evaluated related sensing technologies including tactile sensor array and six DOF force/torque sensor to extract tactile information from breast palpation, where the sensor-tissue interaction of detected palpable lesion can be quantitatively measured and displayed in terms of tactile images. Our laboratory experiments aimed at characterizing the simulated tumors in breast phantom have demonstrated that palpable inclusions can be located to within 1 mm.

Our prototype system incorporates a 3-D Rainbow camera, a tactile sensor array probe, a breast model with simulated lumps, a force/torque sensor on which the breast model is mounted, and a graphical user interface (GUI). Figure 1 shows a block diagram of the tactile mapping device system to be used for measurement of palpable abnormalities in the laboratory. In a typical task, upon detecting a suspicious lump, the examiner will bring the TSAP into contact with the tissue at the palpation site. For a thorough tactile mapping procedure, this involves 3-D positioning the probe through the camera facing the site. The resulting pressure distribution across the probe surface is measured by a Tactile Sensor Array Probe (TSAP) with associated readout electronics. Multiple tactile images with various force levels and torque angles will be required for the lesion characterization. A computer processes the signals to generate appropriate output for visual display on a monitor or raw data to the physician's office through a telecommunication channel. Below, we describe the components of the tactile mapping system.

2.1. 3-D Rainbow Camera

For the accurate positioning of the TSAP, a novel 3-D rainbow camera is adopted in our system, which is suitable for this high-speed 3-D machine vision application. Figure 2 shows the rainbow camera and the acquired sample range image. It exploits a color light projector to illuminate the object in the scene and using an off-the-shelve color camera to obtain a full-frame color image of the scene. The color of the projecting light with spatially continuously varying wavelength is encoded with information of the corresponding projection angle. Each pixel of the color image is associated with a unique ray through the focal point of the camera. Since the angle between camera axis and the ray is known the resulting angle-side-angle triangulation problem can be easily solved when the distance between the light projector and the camera is fixed. Thus, using only one camera, the full frames of 3-D range images can be obtained directly at the camera frame rate. The spatially varying wavelength light is generated by a white light passing through a linear variable wavelength filter. We have performed experiments to investigate the actual range accuracy and the major error contributors. The results show that the 3-D profile of test artifacts were less than 1 mm. The spatial resolution of the system is limited only by the spatial resolution of the camera optical sensing element and is currently able to provide at least

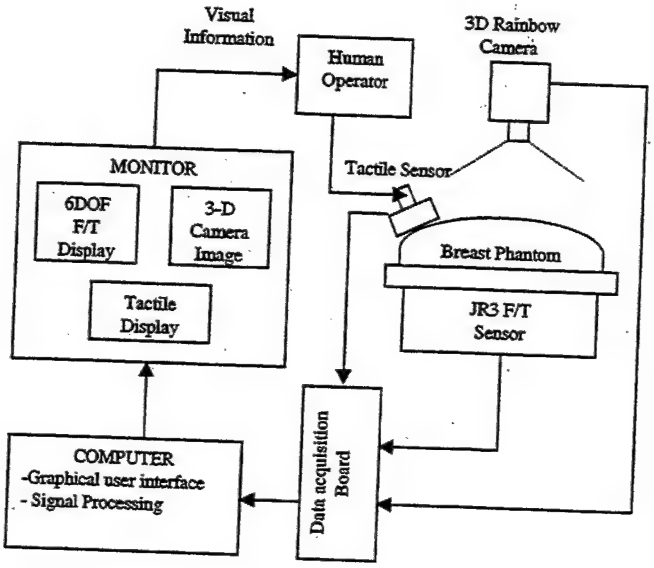

Figure 1: System block diagram of prototype TMD.

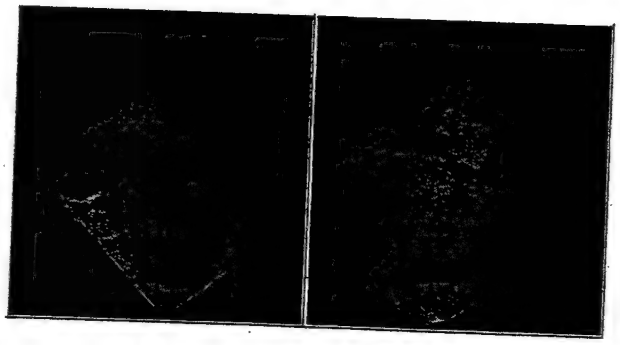

Figure 2: Three-dimentional range image of the breast model by the Rainbow camera.

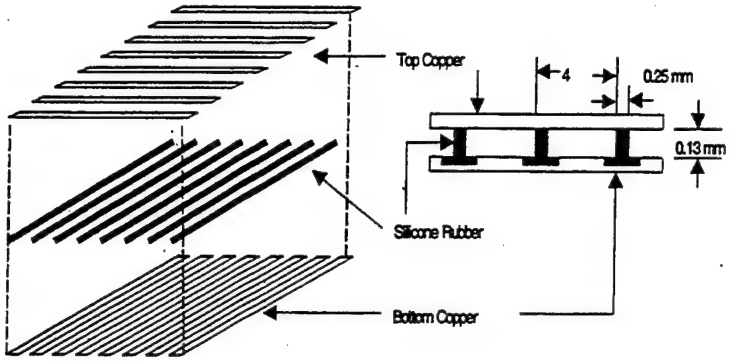

Figure 3: A drawing of a tactile array sensing (adapted from Son 1996).

1024x1024 pixel resolution. When a palpation site is determined, several 3-D range images will be acquired to record the site information.

2.2. Tactile Sensor Array Probe (TSAP)

The core component of the TMD is a highly sensitive tactile sensor array probe. Figure 3 illustrates the operation of the capacitive tactile array sensor used in this system. It shows a drawing of the array with the copper layers and the silicone rubber spacers, which is based on the design by Fearing[6] and Howe.[4] The array is composed of two crossed layers of copper strips separated by thin strips of silicone rubber.[6] Each crossing area forms a capacitor, and when a force is applied onto where the strips cross, the distance between the strips decreases and the capacitance increases.[7] Specially designed electronics will measure the capacitance of each element and relate the capacitance change to the force applied to each element. By measuring the capacitance variations from all the elements simultaneously, we can determine the spatial distribution of pressure across the sensor array.

Figure 4 shows a photograph of a commercial prototype TSAP. The sensor array is made with an inexpensive photolithography and etching process and can be easily attached to a variety of probe shapes. In this prototype specification, it is composed of an eight by eight tactile sensor with elements that are 4 mm on a side. The sensor is mounted on a plastic brass backing plate with a surface that has been machined into a section of a square. The backing plate is 5.08 cm on a side and the effective sensing area is 3.20 cm on a side. We decided to make the sensor flat in order to minimize inhomogeneity because the resulting pressure distribution should have a uniform overall signal to noise ratio. The tactile images will then be consistent when used for various breast/chest background textures. The spatial resolution of the tactile array is 4 mm long where the smallest masses that we are currently interested to characterize are on the order of 1 cm in diameter. Smaller elements would increase spatial resolution at the cost of lower coverage area and low sensitivity since the capacitance is proportional to the element area.[7] The tactile sensor has been shielded to provide electronic insulation.

2.3. Force/Torque Sensing System

The relationship between the hard inclusion (i.e., lump) and the percieved tactile image from the TSAP is nonlinear and complex. In order to characterize and later extract the tactile features of the detected breast lumps, the TMD operation requires that the forces/torques exerted by the operator of the TSAP on the breast model be measured together with the corresponding tactile images. It would be ideal if a force/torque sensor were to be mounted between the wrist and the hand of the operator. Since it is problematic and impractical to mount a force/torque sensor in such a configuration, we decided to mount it under a base which the breast model is placed on. The forces/torques acquired by the sensor in this configuration can be transformed to those exerted by the operator via proper coordinate transformation. Figure 5 shows a breast model laying on a round

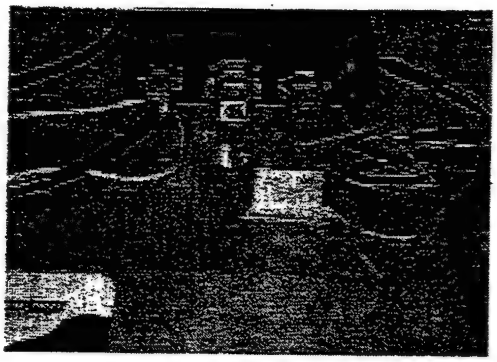

Figure 4: A commercial prototype tactile array sensor probe.

Figure 5: JR^3 Force/Torque Sensor.

base under which a JR^3 force/torque is mounted. The JR^3 force/torque mainly consists of a JR^3 monolithic six DOF force sensor and a JR^3 Intelligent Support System, Comprised of boards for signal conditioning, data acquisition and processing. A computer program was written in Visual C++ to request the JR^3 force/torque sensing system to send to the computer six forces/torques along about the Cartesian x-, y-, z-axes assigned to the base. The transmitting and receiving of data between the computer and the force/torque system is carried out through serial port.

2.4. Breast Models

The breast models used in our laboratory experiments were provided by the HEALTH EDCO, a Division of WRS Group, Inc. The models were made from BIOLIKE^{TM} synthetic tissue that feels just like a real breast [1]. Two models were used in our tests to collect preliminary data. Each of them has 5 lumps that simulate easy- and hard-to-find breast tumors with various sizes and depths at different locations. One of the models is the geriatric breast that is ideally shaped to address the special problems of older women. The geriatric model simulates the natural stretching of the tissue with age. Figure 6 show the distribution of simulated lumps (lesions) in the breast model and the historical spatial distribution of the breast cancer respectively. It should be noticed that as high as 50% of breast cancers occur at the axilia area which is difficult to imaging.

2.5. Graphical User Interface

For both tactile documentation and interactive training, a graphical user interface (GUI) plays a very important role of optimizing both components and examiner's performance. In our prototype, Microsoft Visual C^{++} was employed to implement the GUI to visually display pertinent data of the TSAP and the force/torque sensor. Figure 7 shows the output window of the GUI that presents on-line the pressure distribution acquired by the TSAP, the time response of the 6-DOF force/torque applied by the examiner. The user can interact with the TMD functions through the designed menu

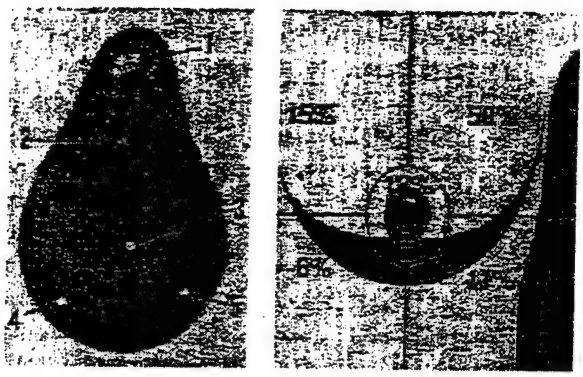

Figure 6. Breast model with simulated lumps (left); and the spatial distribution of the locations of breast cancer occurance (right).

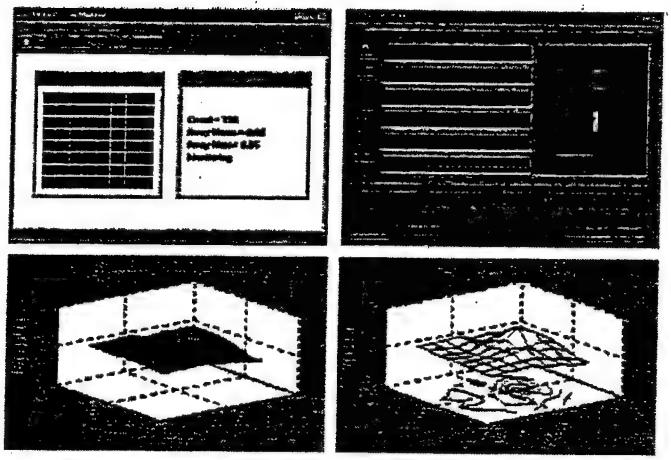

Figure 7. Graphical user interface of the TMD prototype including 6-DOF force/torque feedback (upper left), tactile imaging control menu (upper right), visual display of pressure distribution (lower left), and 3D mesh contour map based localization (lower right).

3. EXPERIMENTAL RESULTS

In order to demonstrate the effectiveness of the TMD system for the characterization and documentation of detected lumps, intensive experiments have been conducted to test the sensitivity and reproducibility of the system in measuring the applied forces and pressure profiles due to lumps. The primary objective here is to quantitatively acquire tactile measurements of the perceived lesions using the TMD system and to evaluate the performance of the system.

During the experiments conducted below, the forces/torques applied by the human examiner during the palpation are recorded in terms of six force parameter values, i.e., Fx, Fy, Fz, Mx, My, Mz. For the tactile imaging of simulated lesions, the TSAP is used to acquire various tactile images by palpating the site after the examiner locates the lesion by initial hand palpation. Since the relationships between the tactile images and lesion characteristics are expected to be complex and nonlinear, we believe that the inverse problem (extraction of lesion characteristics from tactile images) can be solved when sufficient tactile information is acquired. As a result, for each of the lesions, after pushing the TSAP against the breast to achieve certain level of force, the examiner rotates the TSAP to five different orientations at each of which the information about the forces/torques and tactile image are simultaneously recorded. OR1 is the initial orientation of the TSAP after being pushed by the examiner to certain level of force. OR2, OR3, OR4 and OR5 are the TSAP orientations after it is rotated forward, backward, left and right, respectively.

We carry out the above procedure on two different lesions: Lesion 1 and Lesion 4 as identified in Figure 6 (left). Figure 8 shows the 3D mesh surface (left) and the shading interpolation (right) of the pressure distribution measured by the TSAP for Lesion 1, with the top row for OR1 and the following rows for OR2, OR3, OR4 and OR5. Figure 9 shows the results obtained for Lesion 4 presented in the same manner as Figure 8. The values of forces/torques for the experiments conducted for Lesions 1 and 4 are tabulated in Table 1.

Table 1: Results force/torque measurement for Lesion 1 and 4.

Lesion	TSAP Orientation	6DOF Force & Torque (lb./in.lb.)					
		F_x	F_y	F_z	M_x	M_y	M_z
1	OR1	-0.89	0.44	-0.13	-2.58	-10.80	0.50
	OR2	-2.34	2.50	-0.10	-5.26	-22.02	1.59
	OR3	1.69	2.96	-0.03	-2.28	-10.50	3.57
	OR4	3.20	-0.38	0.27	0.40	0.40	2.09
	OR5	-1.83	0.38	-0.03	-2.38	-9.32	1.99
4	OR1	-3.17	1.77	-0.16	5.58	25.59	-0.89
	OR2	-2.08	2.48	-0.22	4.37	18.35	1.78
	OR3	-8.81	-0.03	-0.09	1.98	10.71	0.20
	OR4	-3.67	-1.72	0.00	2.18	10.01	0.39
	OR5	-4.77	4.02	-0.34	3.18	10.81	3.97

Before conducting the experiment on Lesion 1 and Lesion 4, we apply the same procedure on a location at which there exists no lesion. The resulting display shows no peak. Examining the graphical displays in Figure 8 and 9 in comparison with that of the case of no lesion, we notice that a peak consistently occurs in the display. We can draw a preliminary conclusion here that a peak in the graphical display indicates the existence of a lesion. In addition, the force and torque that we recorded in conjunction with the tactile sensing during palpation can give us the information about the contact location and how much force that we apply on the hard lump in the breast model.

4. DISCUSSION AND CONCLUSION

This paper has concerned with the detection of lumps in breast palpation using a tactile mapping device (TMD) system. It presented the main components of the TMD and explained their operations. Experiments were

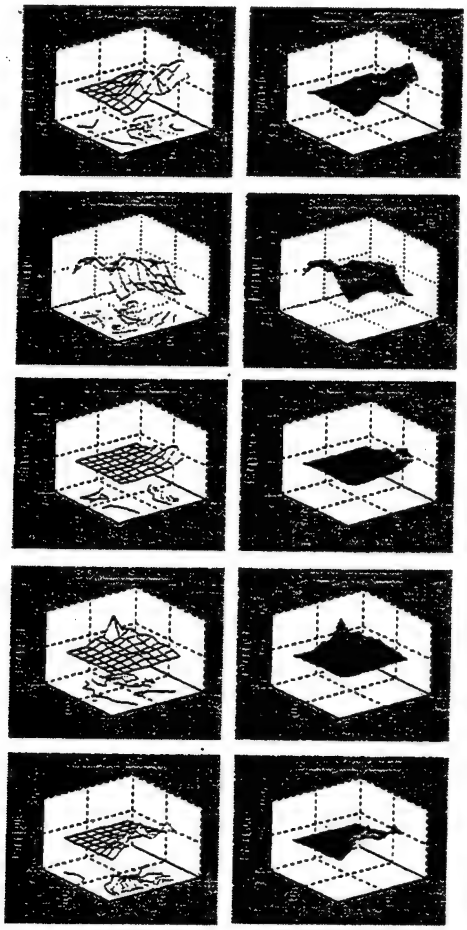

Figure 8: Display of experimental results for lesion 1.

conducted on a breast model to detect two different types of lumps. Experimental data showed that the peak in the display of pressure distribution of the TMD indicated the presence of a lump. The results demonstrated the feasibility of the TMD for improving breast examination technique in diagnosis, documentation, and training. In particular, the results have shown that new tactile mapping technology can quantitatively measure the location and applied forces in breast lumps; the prototype interactive training program can track finger motions and applied forces during breast palpation in which on-line feedback can help the training to better understand the search strategy and adjust force level to increase the sensitivity. With the proven power of nonlinear signal processing using both convolution neural networks (CNN) and multi-layer perceptron (MLP), we expect that the tactile parameters associated with the lesions (i.e., the size and depth of the lesion) can be estimated more accurately than those by the conventional approaches using the first principle of engineering.[7]

ACKNOWLEDGMENTS

This work was supported in part by the US Army Medical Research and Materiel Command under Grants DAMD17-00-0195.

REFERENCES

1. Zeng J., Wang Y., Freedman MT, and Mun SK, "Finger Tracking for Breast Palpation Quantification using Color Image Features," *SPIE J. of Opt. Eng.*, 36(12): 3455-3461, Dec. 1997.

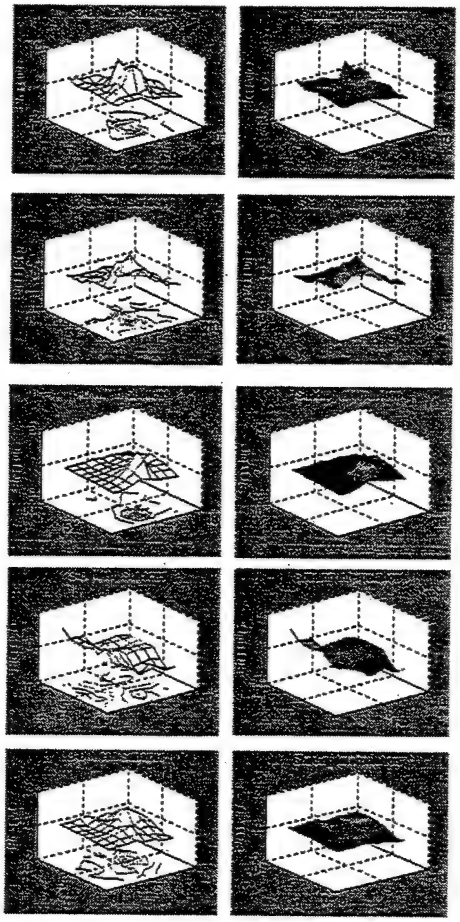

Figure 9: Display of experimental results for lesion 1.

2. Y. Wang, C. Nguyen, R. Srikanchana, J. Geng, and M. T. Freedman, "Tactile Mapping of Palpable Abnormailties for Breast Cancer Diagnosis," *Proc. IEEE Intl. Conf. Robotics and Automation*, Detroit, MI, 1999.
3. Haagensen, CD., Diseases of the Breast, 3rd ed., Philadelphia: Saunders, 1986.
4. Howe, R. D., Peine W. J., Kontarinis, D. A., Son, J., "Remote Palpation Technology," *IEEE Engineering in Medicine and Biology*, 14(3): 318-323, May/June 1995.
5. Dario, P. and Bergamasco, M., "An Advanced Robot System for Automated Diagnosis Tasks through Palpation," *IEEE Trans. Biomed. Eng.*, vol. 35, no. 2, pp.118-126, February 1988.
6. Fearing, R. S., "Tactile Sensing Mechanisms," *Intl. J. Robotics Research*, 9(3): 3-23, 1990.
7. Wellman, P. S., "A Biomechanical Model for tactile Mapping of Palpable Abnormalities," *Harvard Robotics Lab Technical Report* 96-002.
8. Adames, et al., "Lump Detection in Simulated Human Breasts," *Perception and Psychophysics*, 20(3), pp.163, 1976.
9. Fletcher S. W., O'Malley M. S., and Bunce L. A., "Physician's Abilities to Detect Lumps in Silicone Breast Models," *JAMA*, 253(15):2224-2228, 1985.

CLAIMS NOT INCLUDED

PAGES 801 - 922

Mixture of principal axes registration: a neural computation approach

Rujirutana Srikanchana[a], Jianhua Xuan[a], Kun Huang[a], Matthew Freedman[b], and Yue Wang[a]

[a]Department of Electrical Engineering and Computer Science,
The Catholic University of America, Washington, DC 20064, USA
[b]Department of Radiology,
Georgetown University Medical Center, Washington, DC 20007, USA

ABSTRACT

Non-rigid image registration is a prerequisite for many medical imaging applications such as change analysis in image-based diagnosis and therapy assessment. Nonlinear interpolation methods may be used to recover the deformation if the correspondence of the extracted feature points is available. However, it may be very difficult to establish such correspondence at an initial stage when confronted with large and complex deformation. In this paper, a mixture of principal axes registration (mPAR) is proposed to tackle the correspondence problem using a neural computation method. The feature is to align two point sets without needing to establish the explicit point correspondence. The mPAR aligns two point sets by minimizing the relative entropy between their probability distributions resulting in a maximum likelihood estimate of the transformation mixture. The neural computation for the mPAR is developed using a committee machine to obtain a mixture of piece-wise rigid registrations. The complete registration process consists of two steps: (1) using the mPAR to establish an improved point correspondence and (2) using a multilayer perceptron (MLP) neural network to recover the nonlinear deformation. The mPAR method has been applied to register a contrast-enhanced magnetic resonance (MR) image sequece. The experimental results show that our method not only improves the point correspondence but also results in a desirable error-resilience property for control point selection errors.

Keywords: M ixture of Principal Axes Registration, Non-Rigid Image Registration, Change Analysis, Neural Computation, Multilayer Perceptron, Control Points Selection.

1. INTRODUCTION

Image registration is an essential step for many medical image analysis applications such as image fusion, quantitative change analysis in image-based diagnosis and therapy assessment.[1,2] For example, medical diagnosis often benefits from the complementary information in images of different modalities. Multimodality imaging of breast is regarded as a powerful diagnostic tool. In breast imaging, different modalities offer different diagnostic information. In order to fuse the complementary information, the alignment of the images is the first step to be performed to overcome the complication of misregistrations caused by patient motion and physical change. Image registration consists of aligning the images by scaling, rotating, and translating, one or both images so that they are of the same size and have the same orientation and location. Mathematically, image registration can be formulated as to estimate the transformational geometry from two feature point sets, i.e., to recover a matrix representation requiring a set of correspondence matches between features in the two coordinate system. Arun *et. al.*[3] present an algorithm for finding the least-squares solution of the transformation matrix, which is based on the decoupling of translation and rotation and the singular value decomposition (SVD) of a cross-covariance matrix.

Further author information: (Send correspondence to Rujirutana Srikanchana)
E-mail: 55srikanchan@cua.edu, Telephone: 1 202 319 5243
Address: EE/CS Department, The Catholic University of America, Washington, D.C., U.S.A.

Medical Imaging 2002: Image Processing, Milan Sonka, J. Michael Fitzpatrick,
Editors, Proceedings of SPIE Vol. 4684 (2002) © 2002 SPIE · 1605-7422/02/$15.00

The major limitation of the above method is twofold: (1) while feature matching methods can give quite accurate solutions, obtaining correct correspondences of features is a hard problem, especially in the case of images acquired using different modalities or from inter-subjects; and (2) a rigidity assumption is heuristically imposed that is usually not valid in medical images with non-rigid human organs such as breast.[2,4] One popular method that does not require feature correspondence is the principal axes registration (PAR) method.[1] The PAR method is based on the relatively stable geometric properties of image features, i.e., the geometric information contained in these stable image features is often sufficient to determine the transformation between images.[2] However, the PAR method results in a rigid body transform with scaling coefficients. The transform works effectively if the objects to be registered have orientation differences within a certain limit, dependent on the objects' shape and if their shapes are well matched. If their orientations are too different, the transform may arrive at the wrong rotation angle due to problems with object symmetry. Once again, the method cannot handle the cases with non-rigid objects.

In this paper, we present a neural computation based non-rigid image registration method using piecewise rigid transformation. In other words, rather than using a single transformation matrix that gives rise to a large registration error, we attempt to interpolatively apply a mixture of transformations to minimize the registration error. By generalizing PAR to a mixture of principal axes registration (mPAR) scheme, the mixture is fit using the expectation-maximization (EM) algorithm by performing a soft partitioning of the data set. The registration process consists of two steps: (1) using the mPAR to establish an improved point correspondence and (2) using a multilayer perceptron (MLP) neural network to recover nonlinear deformation based on the established point correspondence. A finite mixture of transformations is obtained through aligning the two point sets by minimizing the relative entropy between their probability distributions resulting in a maximum likelihood estimate of the transformation matrix. Specifically, a probabilistic adaptive principal components extraction (PAPEX) algorithm[10] is developed to estimate the transformation matrix using the orthogonal set of eigenvalues and eigenvectors of the auto covariance matrix. A committee machine is then used to combine multiple transformations for the recovery of the total transformational geometry of the non-rigid object. An accurate point correspondence can be established by applying the finite mixture of transformations to the two point sets. Finally, an MLP neural network is adopted to recover the nonlinear deformation by the polynomial mapping function based on the point correspondence.

The mPAR method has been applied to register a contrast-enhanced breast magnetic resonance image (MRI) sequence. With MRI, the breast is usually imaged functionally using a contrast agent. The rate of uptake of the contrast agent is used to characterize a given breast tissue. This rate is studied by observing the change in gray level of the tissue at several instants of time after injection of the agent. However, the non-rigid nature of breast tissue almost guarantees that these different images would be misregistered. To study the uptake process effectively and to also make a quantitative estimate of change in uptake, it would be necessary to align or register these different images. Image registration is thus an important problem. To align these different images, we first extract the control objects of the image using a stochastic segmentation method. With the extracted control objects, we then apply our mPAR method to recover the total transformational geometry of the contrast-enhanced MRI. An accurate point correspondence can be established by applying the mixture of transformations to the two point sets. As a final step, we apply an MLP neural network to recover the nonlinear deformation in the form of the polynomial transformation using the established point correspondence. The experimental results shows that the image differencing after registering two images by applying our mPAR method can greatly improve the accuracy in extraction of the enhanced area compared to that of without any registration.

2. THEORY AND METHOD

Assume two 3-D data point sets $\{\mathbf{p}_{iA}\}$ and $\{\mathbf{p}_{iB}\}$, $i = 1, 2, ..., N$, are related by

$$\mathbf{p}_{iB} = \mathbf{R}\mathbf{p}_{iA} + \mathbf{T} + \mathbf{N}_i \tag{1}$$

where $\mathbf{R}$ is a rotation matrix, $\mathbf{T}$ a translation vector, and $\mathbf{N}_i$ a noise vector. Given $\{\mathbf{p}_{iA}\}$ and $\{\mathbf{p}_{iB}\}$, Arun *et. al.* present an algorithm for finding the least-squares solution of $\mathbf{R}$ and $\mathbf{T}$ by decoupling translation and rotation and using the singular value decomposition (SVD) of a 3×3 cross-covariance matrix.[3]

Suggested by information theory,[5] we can consider the feature point sets in two images as two separate realizations of the same random source. Hence, to align two sets of feature points, we do not need to establish point correspondences to extract the transformation matrix. Instead, we can aligning the two point sets by minimizing the relative entropy between their probability distributions. In other words, if $P_{\{\mathbf{p}_i\}}$ denotes the distribution of the feature point set in an image, we have the simple probabilistic relationship to describe the transformation between two point sets:

$$P_{\{\mathbf{p}_{jB}\}} = P_{\{\mathbf{R}\mathbf{p}_{iA}+\mathbf{T}\}} + \epsilon \tag{2}$$

where ϵ is the noise component. Since the probability distributions can be computed independently on each image without the need to establish feature correspondences, and given the two distributions of the control point sets in the two images, we can recover the transformation matrix in a simple fashion,[2] as we now sketch.

2.1. Registration

For observation of the distributions, we can estimate $\mathbf{R}$ and $\mathbf{T}$ by minimizing the relative entropy (Kullback-Leibler distance) between $P_{\{\mathbf{p}_{jB}\}}$ and $P_{\{\mathbf{R}\mathbf{p}_{iA}+\mathbf{T}\}}$. The least relative entropy estimator is defined as

$$\arg\min_{\mathbf{R},\mathbf{T}} D(P_{\{\mathbf{p}_{jB}\}} || P_{\{\mathbf{R}\mathbf{p}_{iA}+\mathbf{T}\}}) \tag{3}$$

where D denotes the relative entropy measure. Following the same strategy to decouple translation and rotation as in,[3] we can define a new data point by $\mathbf{q}_{iA} = \mathbf{p}_{iA} - \mathbf{p}_A^0$ and $\mathbf{q}_{jB} = \mathbf{p}_{jB} - \mathbf{p}_B^0$, where $\mathbf{p}_A^0$ and $\mathbf{p}_B^0$ are the centroids of $\{\mathbf{p}_{iA}\}$ and $\{\mathbf{p}_{jB}\}$, respectively. Then the optimal geometric transformations, $\mathbf{R}$ and $\mathbf{T}$, can be computed as

$$\mathbf{R} = \mathbf{U}_B \mathbf{H} \mathbf{U}_A^t \tag{4}$$

$$\mathbf{T} = \mathbf{p}_B^0 - \mathbf{R}\mathbf{p}_A^0 \tag{5}$$

where the superscript t denotes matrix transposition, $\mathbf{U}_A$ and $\mathbf{U}_B$ are 3×3 orthonormal matrices, and $\mathbf{H}$ is a 3×3 diagonal matrix with element $h_m = \sqrt{\lambda_{mB}/\lambda_{mA}}$. Note that the transformation $\mathbf{U}$ consists of the orthonormal set of eigenvectors and h_m is the squared root of the eigenvalues λ_m of the auto-covariance matrix $\mathbf{C}$ for $m = 1, 2, 3$ and for $\{\mathbf{p}_{iA}\}$ and $\{\mathbf{p}_{jB}\}$, respectively.

However, because of its global linearity, the application of PAR is somewhat limited to deal with rigid objects only.[6] An alternative paradigm is to model a multimodal control point set with a collection of local linear models. The method is a two-stage procedure: a soft partitioning of the data set followed by estimation of the principal axes within each partition.[7] Recently there has been considerable success in using standard finite normal mixture (SFNM) to model the distribution of a multimodal data set. The association of a SFNM distribution with PAR offers the possibility of being able to register two images through a mixture of probabilistic principal axes transformations.[7] Assume that there are K_0 control point clusters, where each control point cluster defines a transformation $\{\mathbf{R}_k, \mathbf{T}_k\}$. For a point $\mathbf{p}_{nA}$, its new locations corresponding to each of the transformations are $\mathbf{p}_{nk} = \mathbf{R}_k \mathbf{p}_{nA} + \mathbf{T}_k$ for $k = 1, ..., K_0$. Further assume that the control point set defines a SFNM distribution

$$f(\mathbf{p}_i) = \sum_{k=1}^{K_0} \pi_k g(\mathbf{p}_i | \mu_k, \mathbf{C}_k) \tag{6}$$

where g is the Gaussian kernel with mean vector μ_k and auto-covariance matrix $\mathbf{C}_k$, and π_k is the mixing factor proportional to the number of control points in cluster k. For each of the control point sets $\{\mathbf{p}_{iA}\}$ and $\{\mathbf{p}_{iB}\}$, the mixture distribution is fit using the expectation-maximization (EM) algorithm. In principle, the E step involves assigning to the linear models responsibilities, i.e., the posterior Bayesian probability, from the control points; the M step involves re-estimating the parameters of the linear models from the above assignment.[7]

Thus the statistical membership of point $\mathbf{p}_{nA}$ belonging to each of the control point clusters can be derived by

$$z_{nk} = P(\mathbf{R}_k, \mathbf{T}_k | \mathbf{p}_{nA}) = \frac{\pi_{kA} g(\mathbf{p}_{nA} | \mu_{kA}, \mathbf{C}_{kA})}{f(\mathbf{p}_{nA})} \tag{7}$$

i.e., the posterior probability of $\{\mathbf{R}_k, \mathbf{T}_k\}$ given $\mathbf{p}_{nA}$. We can define the mPAR transformation as

$$\mathbf{p}_n = \sum_{k=1}^{K_0} z_{nk}\mathbf{p}_{nk} \tag{8}$$

$$= \sum_{k=1}^{K_0} \frac{\pi_{kA}\, g(\mathbf{p}_{nA}|\mu_{kA}, \mathbf{C}_{kA})}{f(\mathbf{p}_{nA})}(\mathbf{R}_k\mathbf{p}_{nA} + \mathbf{T}_k) \tag{9}$$

where $\{\mathbf{R}_k, \mathbf{T}_k\}$ is determined based on $\{\mu_{kA}, \mathbf{C}_{kA}\}$and $\{\mu_{kB}, \mathbf{C}_{kB}\}$, which we have estimated in the previous step using the EM algorithm. This philosophy for recovering transformational geometry of the non-rigid objects is similar in spirit to the *divide-and-conquer* principle,[6] under which the relative entropy between the two point sets reaches its minimum

$$\arg\min_{\mathbf{R}_k, \mathbf{T}_k} D(P_{\{\mathbf{p}_{jB}\}}||P_{\{\sum_{k=1}^{K_0} z_{ik}(\mathbf{R}_k\mathbf{p}_{iA}+\mathbf{T}_k)\}}) \tag{10}$$

both globally and locally.

Based on a mixture of probabilistic principal axes transformations, the next section describes a neural computation using a committee machine to obtain a mixture of piece-wise rigid registrations, which gives a reliable point correspondence using multiple extracted object control points.

2.2. Neural Computation

There are many numerical techniques to perform the maximum likelihood estimation. The most popular method is the EM algorithm. The EM algorithm first calculates the posterior Bayesian probabilities of the data through the data observations and the current parameter estimates (E-Step) and then updates parameter estimates (M-Step). The procedure cycles back and forth between these two steps. A neural network interpretation of the EM algorithm is given in.[8] Because of its reputation of being slow in which new information acquired in the expectation step is not used immediately, on-line versions of the EM algorithm are proposed for large-scale sequential learning. We adopt a fully unsupervised and incremental stochastic learning algorithm to implement the EM algorithm. The scheme provides winner-takes-in probability (Bayesian "soft") splits of the control points, hence allowing the data to contribute simultaneously to multiple clusters. The incremental stochastic learning EM algorithm can be described as follows:

E − Step

$$z_{(i+1)k} = \frac{\pi_k^{(i)} g(\mathbf{p}_{i+1}|\mu_k^{(i)}, \mathbf{C}_k^{(i)})}{f(\mathbf{p}_{i+1}|\pi_k^{(i)}, \mu_k^{(i)}, \mathbf{C}_k^{(i)})} \tag{11}$$

M − Step

$$\mu_k^{(i+1)} = \mu_k^{(i)} + a(i)(\mathbf{p}_{i+1} - \mu_k^{(i)})z_{(i+1)k}, \tag{12}$$

$$\mathbf{C}_k^{(i+1)} = \mathbf{C}_k^{(i)} + b(i)[(\mathbf{p}_{i+1} - \mu_k^{(i)})(\mathbf{p}_{i+1} - \mu_k^{(i)})^T - \mathbf{C}_k^{(i)}]z_{(i+1)k}, \tag{13}$$

$$\pi_k^{(i+1)} = \frac{i}{i+1}\pi_k^{(i)} + \frac{1}{i+1}z_{(i+1)k} \tag{14}$$

for $k = 1, ..., K_0$ and for $\{\mathbf{p}_{iA}\}$ and $\{\mathbf{p}_{iB}\}$, respectively. In the above equations, $a(i)$ and $b(i)$ are introduced as the learning rates that converge to zero, ensuring unbiased estimates after convergence. This procedure is termed as neural computation of the EM algorithm. At each complete cycle of the algorithm, we first use "*old*" set of parameter values to determine the posterior probabilities $z_{(i+1)k}$. These posterior probabilities are then used to obtain "*new*" values $\pi_k^{(i+1)}, \mu_k^{(i+1)}, \mathbf{C}_k^{(i+1)}$. The algorithm cycles back and forth until the value of relative entropy between the data histogram and mixture model reaches its minimum

$$\arg\min_{\pi_k, \mu_k, \mathbf{C}_k} D(P_{\{\mathbf{p}_i\}}||f(\mathbf{p}_i)) \tag{15}$$

for $\{\mathbf{p}_{iA}\}$ and $\{\mathbf{p}_{iB}\}$, respectively.

With a soft partitioning of the data set using Eqs. (11-14), control points will now effectively belong to more than one cluster spatially. Thus, the effective input values are $\mathbf{p}_{ik} = z_{ik}(\mathbf{p}_i - \mu_k)$ for an independent registration transformation k in the committee machine.[9] We then extend an adaptive principal components extraction (APEX) algorithm to a probabilistic version, i.e., PAPEX,[10] to determine $\mathbf{U}_k$ for $\{\mathbf{p}_{iA}\}$ and $\{\mathbf{p}_{iB}\}$, respectively, summarized as follows.

1. Initialize the feedforward weight vector $\mathbf{u}_{mk}$ for $m = 1, 2, 3$, and the feedback weight vector $\mathbf{a}_{mk}$ to small random values for $m = 2, 3$, at time $i = 1$. Assign a small positive value to the learning rate parameter η.

2. Set $m = 1$, and for $i = 1, 2, ...,$ compute

$$y_{1k}(i) = \mathbf{u}_{1k}^T(i) z_{ik}(\mathbf{p}_i - \mu_k) \tag{16}$$

$$\mathbf{u}_{1k}(i+1) = \mathbf{u}_{1k}(i) + \eta[y_{1k}(i) z_{1k}(\mathbf{p}_i - \mu_k) - y_{1k}^2(i)\mathbf{u}_{1k}(i)] \tag{17}$$

   For large i we have $\mathbf{u}_{1k}(i) \longrightarrow \mathbf{u}_{1k}$, where $\mathbf{u}_{1k}$ is the eigenvector associated with the largest eigenvalue of the cluster k, and $\lambda_{1k} = \frac{1}{N}\sum_{i=1}^{N} y_{1k}^2(i)$.

3. Set $m = 2$, and for $i = 1, 2, ...,$ compute

$$\mathbf{y}_{(m-1)k}(i) = [y_{1k}(i), y_{2k}(i), ..., y_{(m-1)k}(i)]^T \tag{18}$$

$$y_{mk}(i) = \mathbf{u}_{mk}^T(i) z_{ik}(\mathbf{p}_i - \mu_k) + \mathbf{a}_{mk}^T(i)\mathbf{y}_{(m-1)k}(i) \tag{19}$$

$$\mathbf{u}_{mk}(i+1) = \mathbf{u}_{mk}(i) + \eta[y_{mk}(i) z_{ik}(\mathbf{p}_i - \mu_k) - y_{mk}^2(i)\mathbf{u}_{mk}(i)] \tag{20}$$

$$\mathbf{a}_{mk}(i+1) = \mathbf{a}_{mk}(i) - \eta[y_{mk}(i)\mathbf{y}_{(m-1)k}(i) + y_{mk}^2(i)\mathbf{a}_{mk}(i)] \tag{21}$$

   For large i we have $\mathbf{u}_{2k}(i) \longrightarrow \mathbf{u}_{2k}$, where $\mathbf{u}_{2k}$ is the eigenvector associated with the second largest eigenvalue of the cluster k, and $\lambda_{2k} = \frac{1}{N}\sum_{i=1}^{N} y_{2k}^2(i)$.

4. Set $m = 3$, go to step 3. For large i we have $\mathbf{u}_{3k}(i) \longrightarrow \mathbf{u}_{3k}$, where $\mathbf{u}_{3k}$ is the eigenvector associated with the third largest eigenvalue of the cluster k, and $\lambda_{3k} = \frac{1}{N}\sum_{i=1}^{N} y_{3k}^2(i)$. The next step is to introduce a committee machine for combining multiple transformations in a mixture fashion.

Consider the modular network nature of Eq. (8), we can easily realize that it is a mixture of local expert model. Each local expert performs supervised learning through our PAPEX algorithm, and the individual responses of the experts are nonlinearly combined by means of a single gating network. This is our committee machine to combine multiple transformations to form the total transformational geometry of the non-rigid object. The neural computation of a committee machine can be achieved by distributing the learning tasks among a number of experts, which in turn partitioning the input space into a set of subspaces. The experts are in theory performing supervised learning in that the individual outputs are combined to model the desired response. There is, however, a sense in which the experts are also performing self-organized learning; that is, they self organize to find a good partitioning of the input space so that each expert does well at modeling its own subspace, and as a whole group they model the input space jointly. It is assume here that the different experts work best in different regions of the input space in accordance with the probabilistic generative model. In our case, the effective input values are $\mathbf{p}_{ik} = z_{ik}(\mathbf{p}_i - \mu_k)$ for an independent registration transformation k in the networks. A committee machine consists of k supervised modules, with a soft partitioning of the data set using EM algorithm and the function PAPEX to determine the transformation of the orthogonal set of eigenvalues and eigenvectors of the auto-covariance matrix among the networks. The output of an integrating unit in our committee machine is a transformational matrix of the image pair.

Based on those correspondences established by applying the transformational matrix between the two images, the control points of two images are obtained. The final step is to recover the deformation of the object by calculating the polynomial transformation using piece-wise interpolation. The goal is to fine tune the alignment

achieved in the initial registration by considering the object as a non-rigid body. This allows for the consideration of the non-rigid deformation between the images. The polynomial based transform such as thin-plate spline (TPS) has been shown to be able to handle non-rigid deformations of the object. In our case, we develop a three-layer MLP neural network to acquire the polynomial transform, where the input nodes are fed with the coordinates of the corresponding control points of the image. The MLP is trained by the corresponding control point pairs as its inputs and outputs using the backpropagation algorithm. The three-layer MLP converges to a polynomial transform that captures the relationship between corresponding control point pairs. The MLP neural network further recovers the underlying non-linear deformation between two images by interpolating the learned relationship between corresponding control point pairs. Finally, by applying the MLP polynomial transform to all the pixels in an image followed by a bilinear grey level interpolation method, we can obtain all the pixel intensity values in the image that is our final registered image.

In order to apply our registration method, we need to establish the corresponding objects between two images. We have developed a stochastic segmentation method to extract the corresponding objects in both images. The mPAR uses these corresponding objects to combine multiple transforms recovered by PAR in a mixture form. After the mPAR step, we can easily establish control point correspondence where control points are selected corner points on the boundaries of extracted corresponding objects. Next, we will describe our segmentation method for control point extraction.

2.3. Segmentation

Assume that each pixel in the image can be decomposed into pixel images x and context image l. By ignoring information regarding the spatial ordering of pixels, we can treat context images as random variables and describe them using a multinomial distribution with unknown parameters π_k, $k = 1, ..., K$, which can be interpreted as a prior probability of pixel labels determined by the global context information. In particular, based on the statistical properties of pixel images, where pixel image is defined as the observed gray level associated with the pixel, a SFNM distribution is justified to model the image histogram by determining the optimal parameters with respect to a distance measure of a sum of the following general form $f_\tau(x) = \sum_{k=1}^{K} \pi_k g(x|\mu_k, \sigma_k^2)$ with $\sum_{k=1}^{K} \pi_k = 1$, $\pi_k \geq 0$, and $g(x|\mu_k, \sigma_k^2) = \frac{1}{\sqrt{2\pi}\sigma_k} \exp(-\frac{(x-\mu_k)^2}{2\sigma_k^2})$ where μ_k and σ_k are the mean and variance of the k^{th} Gaussian kernel, and π_k is the global regularization parameter. We use K to denote the number of Gaussian components and τ to denote the parameter vector. This tissue quantification is achieved through three completely unsupervised steps: (1) parameter initialization by optimal histogram quantization, (2) model estimation by histogram based fast EM algorithm, and (3) model selection by minimum description length (MDL) criterion. It is shown that the SFNM model converges to the true distribution when the pixel image are asymptotically independent.[17]

After we obtain the optimal parameters for all components, we use a multiple thresholding procedure for initializing image segmentation based on maximum likelihood (ML) principle, which is followed by contextual Bayes relaxation labeling (CBRL) algorithm to obtain a consistent labeling solution based on localized SFNM formulation for improving initial segmentation by using neighborhood text regularities. We define the component in localized SFNM by the support function:

$$S_i(k) = \pi_k^{(i)} \frac{1}{\sqrt{2\pi}\sigma_k} \exp(-\frac{(x-\mu_k)^2}{2\sigma_k^2}) \tag{22}$$

where $\pi_k^{(i)}$ is the local conditional prior of regions, the support function $S_i(k)$ is a function of the component (tissue type) k. Then tissue segmentation is interpreted as the satisfaction of a system of inequalities as follows $S_i(l_i) \geq S_i(k)$ for all k and for $i = 1, ..., N$, where $l_i, i = 1, ..., N$ is the context images, and a consistent labeling is defined as the one having maximum support at each pixel simultaneously. We further define the average local consistency measure $A(l) = \sum_{i=1}^{N} \sum_k I(l_i, k) S_i(k)$ to link consistent labeling to global optimization.[18]

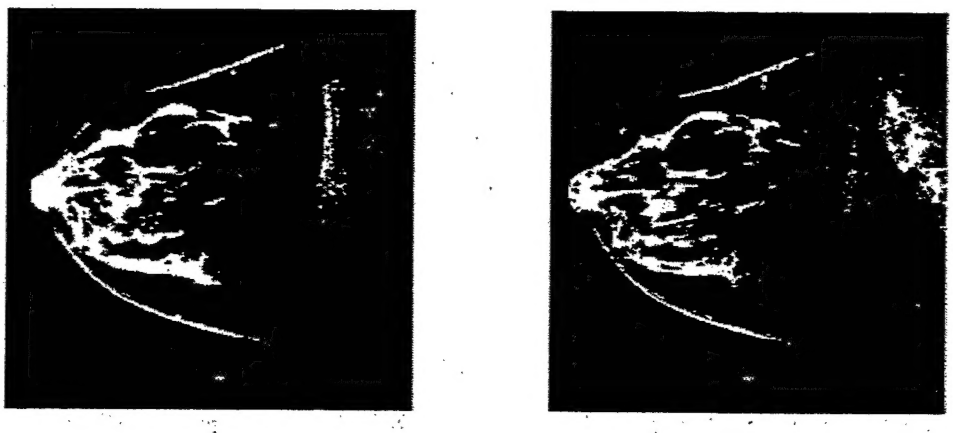

Figure 1: Segmentation result of fibroglandular tissue (left: pre-contrast image; right: post contrast image).

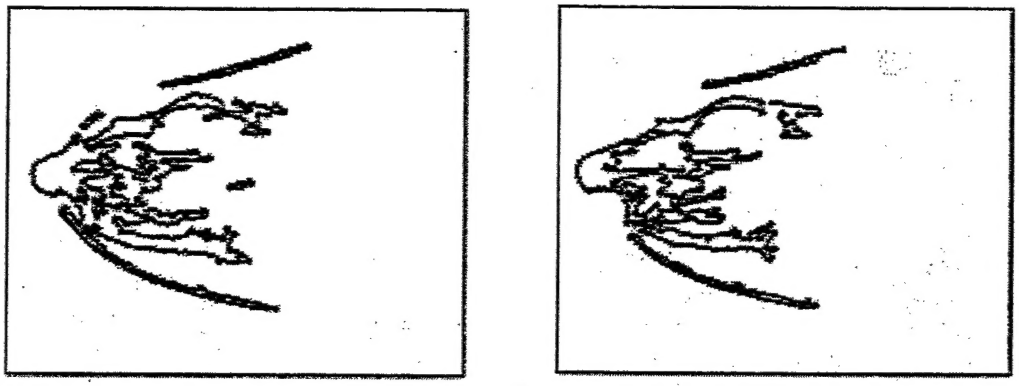

Figure 2: Extracted control points in a pre-contrast image (left) and a post-contrast image (right).

3. RESULT AND DISCUSSION

We applied our mPAR method to register pre- and post-contrast MR breast images. A 3-D breast MRI scan is acquired prior to the injection of contrast agent, followed by a sequence of 3-D breast MRI scan after the agent has been applied. The goal of image registration for this study is to relate any point in the post-contrast sequence to the pre-contrast reference image. The first step of our method is try to correct the global misalignment by performed a pre-registration step using the PAR method. The PAR method uses the extracted skinline as the control objects to globally align images. Since we do not want to change any contents in the post-contrast image, we decide to apply our registration method to the pre-contrast image. After we performed the pre-registration step, we applied our segmentation method to extract the control objects (fibroglandular tissue) in both pre- and post-contrast images. Figure 1 shows the segmented regions of fibroglandular tissue that will be used in our mPAR method as the corresponding control objects for non-rigid registration.

Our mPAR method treats the regions of fibroglandular tissue as multiple objects that can be obtained using the EM soft-partitioning algorithm. We then apply the PAPEX algorithm to determine transformation matrices between all the corresponding objects. A committee machine is then used to combine individual transforms to form a total transformational geometry of the non-rigid object, i.e., resulting in a mixture of individual transforms. After we apply the mixture transformation matrix to pre-contrast image, all the objects (i.e., the regions of fibroglandular tissue) are well aligned. We then apply a corner detection algorithm to extract those high-curvature points on the boundaries of fibroglandular tissue to serve as control points for the

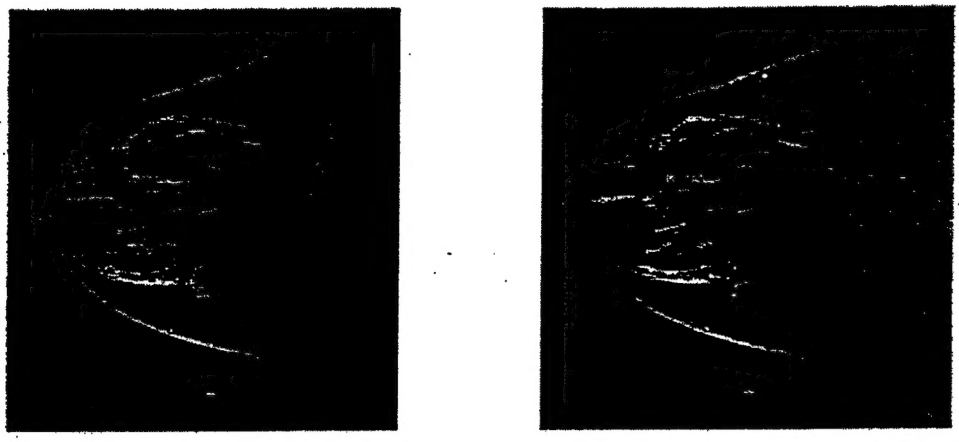

Figure 3. A pair of a contrast-enhanced breast MR images (left: pre-contrast image with global alignment based on PAR method; right: post contrast image).

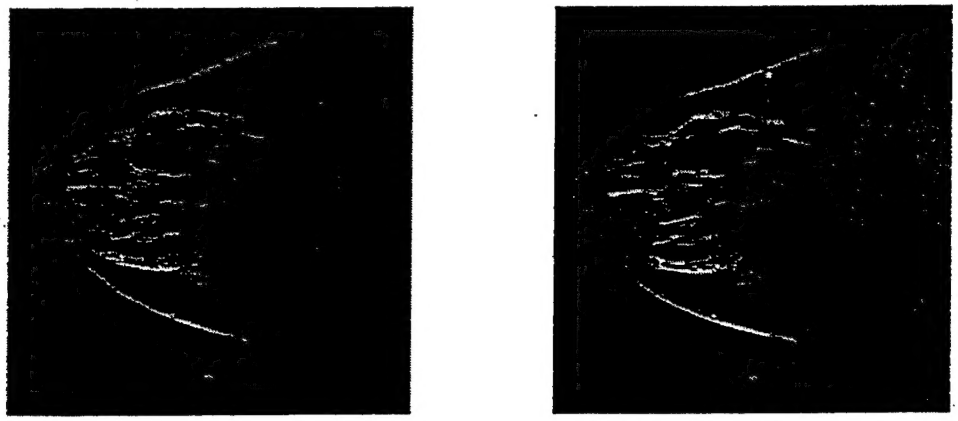

Figure 4. A pre-contrast image (left) and a registered post-contrast (right) image using the mPAR registration method.

MLP. Figure 2 shown the extracted control points in both pre- and post-contrast images. The control point correspondence between pre- and post-contrast images can be conveniently established using a simple correlation method. Finally, an MLP neural network is trained using the corresponding control point pairs to recover the nonlinear deformation between two images. The non-linear deformation is represented by a polynomial mapping function that is interpolated by the neural network based on the control point correspondence. Figure 4 shows a registered pre- and post-contrast image pair using our non-rigid registration method - the mPAR method.

To relate a post-contrast image to a pre-contrast image, we simple do the image difference between the post-contrast image and the pre-contrast image. The difference results are the enhanced area of fibroglandular tissue, i.e., the area that has been highlighted by the contrast agent. Figure 5 (left) shows the difference images between the post-contrast image and registered pre-contrast image. As a comparison, we also show the difference image of the post-contrast image and unregistered (original) pre-contrast image in Figure 5 (right), where false regions of the enhanced area of fibroglandular tissue can be observed due to the misalignment between pre- and post contrast images. The results demonstrate that the mPAR can successfully recover the deformation between pre- and post-contrast images so the enhanced area can be accurately extracted by image differencing between the post-contrast image and registered pre-contrast image.

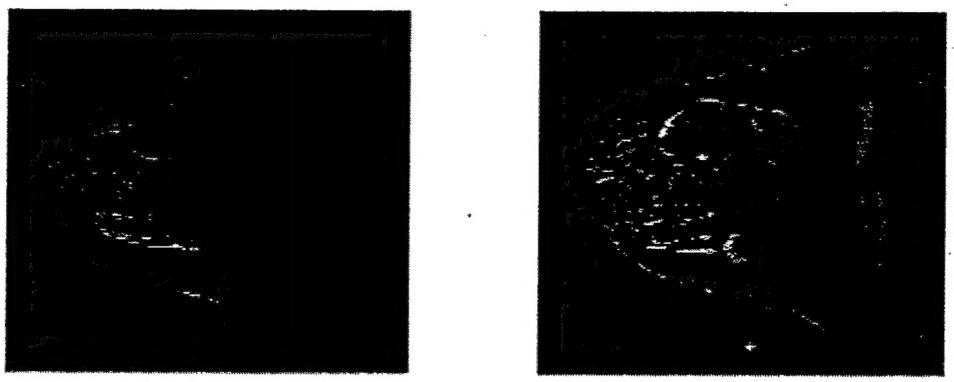

Figure 5. Difference images of the enhanced area (left: difference image with our mPAR registration; right: difference image without registration).

4. CONCLUSION

In this paper, we have presented the theoretical concepts and methods of a neural computation based non-rigid image registration method - the mPAR method. The approach uses a committee machine to recover the total transformational geometry of the non-rigid object. The committee machine combines multiple rigid transforms in a finite mixture registration scheme. Finite mixture transform combination is a novel technique to combine multiple transforms contained in a single image, which yields a lower mean square error (MSE) than that of using any local transform alone. In other word, the mPAR method results in a smooth image while local transforms yield an image containing discontinuities on transform boundaries. In addition, the registration obtained by the committee machine is fine tuned using the nonlinear transform recovered by a MLP network. The MLP neural network is trained by the extracted control point pairs and converges to a polynomial transform that captures the nonlinear deformation between two images.

We have applied our mPAR algorithm to MR breast registration problem. The experimental results have demonstrated that our mPAR method can successfully recover the nonlinear deformation between images. More importantly, our mPAR method aligns two point sets without the need of establishing explicit point correspondence. Instead, it aligns the two point sets by minimizing the relative entropy between their probability distributions. Furthermore, through aligning the two point sets initially by our mPAR method, we can improve the accuracy of establishing the feature point correspondence. The MLP neural network has been introduced to recover the deformation based on established feature point correspondence. The MLP has also resulted in a desirable error-resilience property for control point selection errors. However, some distortion can be observed in the final warped images. We believe that the distortion is largely caused by the errors in control point selection and correspondence. Improvement in this portion should reduce the distortion and yield better registration results. Finally, it is worthy noting that using neural networks in this problem has increased the generality of this approach to allow us to improve the algorithm and adjust performance as imaging conditions change.

ACKNOWLEDGMENTS

This work was supported by the US Army Medical Research and Materiel Command under Grants DAMD17-00-0195 and DAMD17-98-8045.

REFERENCES

1. M. Moshfeghi and H. Rusinek, "Three-dimensional registration of multimodality medical images using the principal axes techniques," *Philips J. Res.*, vol. 47, no.2, pp. 81-97, 1992.

2. V. Govindu and C. Shekhar, "Alignment using distributions of local geometric properties," *IEEE Trans. Pattern Anal. Machine Intell.*, vol. 21, no.10, pp. 1031-1043, October 1999.
3. K. S. Arun, T. S. Huang, and S. D. Blostein, "Least-squares fitting of two 3-D point sets," *IEEE Trans. Pattern Anal. Machine Intell.*, vol. 9, no.5, pp. 698-700, September 1987.
4. A. D.J. Cross and E. R. Hancock, "Graph matching with a dual-step EM algorithm," *IEEE Trans. Pattern Anal. Machine Intell.*, vol. 20, no.11, pp. 1236-1253, November 1998.
5. T. M. Cover and J. A. Thomas, *Elements of Information Theory*, New York: Wiley, 1991.
6. G. E. Hinton, P. Dayan, and M. Revow, "Modeling the manifolds of images of handwritten digits," *IEEE Trans. Neural Nets.*, vol. 8, no.1, pp. 65-74, January 1997.
7. Y. Wang, L. Luo, M. T. Freedman, and S. Y. Kung, "Probabilistic principal component subspaces: A hierarchical finite mixture model for data visualization," *IEEE Trans. Neural Nets.*, vol. 11, no. 3, pp. 625-636, May 2000.
8. L. Perlovsky and M. McManus, "Maximum likelihood neural networks for sensor fusion and adaptive classification," *Neural Networks*, vol. 4, pp. 89-102, 1991.
9. S. Haykin, Neural Networks: A Comprehensive Foundation, 2nd ed., Prentice-Hall, Inc., Upper Saddle River, Ney Jersey, 1999.
10. S. Y. Kung, *Principal Component Neural Networks*, New York: Wiley, 1996.
11. M. I. Jordan and R. A. Jacobs, "Hierarchical mixture of experts and the EM algorithm," *Neural Computation*, vol. 6, pp. 181-214, 1994.
12. D. M. Titterington, A. F. M. Smith, and U. E. Markov, *Statistical analysis of finite mixture distributions*, New York: John Wiley, 1985.
13. K. Woods, et. al., "Patient site model supported change detection," *Proceedings of SPIE Medical Imaging: 2000*, vol.1, no. 24 , pp. 1095-1106, 2000.
14. J. Lu, R. Srikanchana, M. McClain, Y. Wang, J. Xuan, I. A. Sesterhenn, M. T. Freedman, and S. K. Mun, "A statistical volumetric model for characterization and visualization of prostate cancer," *Proc. SPIE Medical Imaging*, vol. 3976, pp. 142-153, 2000.
15. K. Woods, *Image Guided Diagnosis through Change Detection in Image Sequences*, Doctoral Dissertation, The Catholic University of America, 2000.
16. P. Santago and H.D. Gage, "Quantification of MR Brain images by mixture density and partial volume modeling," *IEEE Trans. Med. Imag.*, vol. 12, no. 3, pp. 566-574, Sept. 1993.
17. Y.Wang and T. Adali, "Efficient learning of finite normal mixtures for image quantification," *Proc. IEEE Int. Conf. Acoustic, Speech, and Signal Processing*, Atlanta, GA, 1996, pp. 3422-3425.
18. R. A. Hummel and S. W. Zucker, "On the foundations of relaxation labeling processes," *IEEE Trans. Pattern Anal. Machine Intell.*, vol. 5, May 1983.